LIST OF PUBLICATIONS

1) Yaowamarn Chuminjak, Suphaporn Daothong, Preeyaporn Reanpang, Johannes Philipp Mensing, Ditsayut Phokharatkul, Jaroon Jakmunee, Anurat Wisitsorrat, Adisorn Tuantranont and Pisith Singjai, “Electrochemical Energy-Storage Performances of Nickel Oxide Films Prepared by Sparking Method”, RSC Advances, 5, 2015 , 67795-67802.
2) Yaowamarn Chuminjak, Suphaporn Daothong, Aekapong Kuntarug, Ditsayut Phokharatkul, Mati Horprathum, Anurat Wisitsoraat, Adisorn Tuantranont, Jaroon Jakmunee and Pisith Singjai, “ High-performance Electrochemical Energy Storage Electrodes Based on Nickel Oxide-coated Nickel Foam Prepared by Sparking Method”, 238, 2017, Pages 298-30.

Appendices

APPENDIX A

Yaowamarn Chuminjak, Suphaporn Daothong, Preeyaporn Reanpang, Johannes Philipp Mensing, Ditsayut Phokharatkul, Jaroon Jakmunee, Anurat Wisitsorrat, Adisorn Tuantranont and Pisith Singjai, "Electrochemical Energy-Storage Performances of Nickel Oxide Films Prepared by Sparking Method", RSC Advances, 5, 2015, 67795-67802.

RSC Advances

PAPER

Cite this: *RSC Adv.*, 2015, **5**, 67795

Electrochemical energy-storage performances of nickel oxide films prepared by a sparking method

Yaowamarn Chuminjak,[a] Suphaporn Daothong,[b] Preeyaporn Reanpang,[c] Johannes Philipp Mensing,[d] Ditsayut Phokharatkul,[d] Jaroon Jakmunee,[c] Anurat Wisitsoraat,[d] Adisorn Tuantranont[d] and Pisith Singjai*[a]

Received 20th May 2015
Accepted 28th July 2015

DOI: 10.1039/c5ra09408a

www.rsc.org/advances

In this work, nickel oxide (NiO) films have been prepared by a sparking method on flexible chromium/gold coated polyethylene terephthalate substrates and investigated for electrochemical energy-storage applications. Structural characterizations by scanning/transmission electron microscopies, X-ray diffraction, X-ray photoelectron spectroscopy and a UV-vis spectrophotometer reveal that the film comprises polycrstalline NiO nanoparticles with diameters in the range of 3.0–6.0 nm loosely agglomerated into a porous foam-like network. The nanoporous sparked NiO films, exhibit remarkable energy-storage behavior with a high average specific charge capacity of 402.75 C g^{-1} at a discharge current of 1 A g^{-1} and a good capacity retention of 88% after 1000 cycles at a high discharge current of 40 A g^{-1}. Thus, the sparking method is a promising alternative route for the preparation of high-performance electrochemical energy-storage devices.

Introduction

Recently, transition metal oxide (TMO) nanoparticles have been widely studied for energy-storage applications including fuel cells, electrochromic capacitors and batteries because of their advantageous properties including high specific surface area, high electrocatalytic activity and good structural stability.[1–4] In electrochemical energy-storage applications, TMOs such as RuO_2, V_2O_5, Fe_3O_4, MnO_2 and NiO have been shown to exhibit promising performances with high specific capacitances and high energy densities owing to their excellent charge storage characteristics.[5–9] Among various TMO, NiO is a particularly attractive choice[10–16] because of its exceptionally high theoretical specific capacitance (3750 F g^{-1}), excellent redox activity, low toxicity, low cost, and environmental friendly nature.[11–13] The performances of NiO-based electrochemical energy-storage devices are related to its structural, chemical and electrical properties, which depend considerably on the preparation method. NiO has been synthesized by a variety of chemical and physical approaches.[14,15,17–22] Chemical methods including chemical bath deposition, electrodeposition, chemical precipitation, spray pyrolysis, hydrothermal process and sol gel process usually generate harmful chemical wastes or excess chemical impurities, which come from the chemical precursors or other chemical agents used in the processes. Physical methods such as thermal decomposition/oxidation, thermal evaporation and pulsed laser deposition can avoid these shortcomings. However, most of them require either high vacuum system or high-temperature operation, which are expensive and impractical for low-cost energy-storage applications. In addition, the high temperature requirement complicates its use and application with other low-temperature components such as plastic substrates.

Therefore, an alternative physical synthesis method should be developed to achieve NiO nanostructures with high pseudo-capacitive characteristics at low cost and low temperature. Sparking technique is a fairly new fabrication process that can create porous nanostructured films of metal and metal oxide with uniform composition and well-controlled thickness in one step at low cost.[23–25] It utilizes arcing between two metal tips to form nanoparticulate films under atmospheric condition so that an expensive vacuum system is not required and it can be easily scaled up for commercial use. Recently, various metal oxide nanoparticle films including TiO_2, ZnO and In_2O_3 have been prepared by sparking method and applied for photo-catalysts, double-layered photoelectrodes in dye-sensitized solar cells and gas sensors.[23–25] However, there is no report of NiO nanostructured films prepared by the sparking method for energy-storage applications. In this work, NiO films are deposited by the sparking method and its electrochemical energy-

[a]*Deparment of Physics and Materials Science, Faculty of Science, Chiang Mai University, Chiang Mai, 50200, Thailand. E-mail: pisith.s@cmu.ac.th; Fax: +66-538-922-70; Tel: +66-538-922-71*

[b]*Program in Materials Science, Faculty of Science, Maejo University, Chiang Mai, 50290, Thailand*

[c]*Research Laboratory for Analytical Instrument and Electrochemistry Innovation, Faculty of Science, Chiang Mai University, Chiang Mai 50200, Thailand*

[d]*Nanoelectronics and MEMS Laboratory, National Electronics and Computer Technology Center (NECTEC), 112 Paholyothin Rd., Klong1, Klong Luang, Pathumthani, 12120, Thailand*

storage performances are investigated by cyclic voltammetry (CV) and galvanostatic charge–discharge (GCD) measurements.

Materials and methods

The schematic illustration of the sparking apparatus for the fabrication of NiO nanoparticles (NiO-NPs) and NiO films is shown in Fig. 1. Nickel is sparked off between nickel anode and cathode tips under a high applied voltage onto a substrate placed directly below the wires. The sparking machine was equipped with an array of nickel electrodes that would be scanned in one dimension while the substrate would be sliding automatically in another dimension with controllable rates by step motors. The design of sparking system allowed rapid deposition of nanoparticle films over a large area and improved the uniformity and quality of these films. Nickel wires (99.98%, Advent Research Material Ltd, Oxford, UK) with 0.25 mm in diameter were used as the anode and cathode electrodes. Before use, nickel wires were washed with acetone, absolute ethanol, and de-ionized water in an ultrasound bath for 15 min and then dried by nitrogen gas at room temperature. The wires were cut to form sparking tips and then aligned with a gap between anode and cathode of ~1 mm. The NiO films as working electrodes were deposited by direct sparking from an array of nickel wires at 3 kV and 10 mA onto chromium/gold (Cr/Au) current collector layers on flexible polyethylene terephthalate (PET) substrates. The high applied voltage induced high-temperature arcing plasma in the air gap *via* field ionization process. Electrons and ions in the plasma bombarded at the two tip surfaces, producing vaporized nickel nanoparticles that were oxidized in air at the high plasma temperature into NiO-NPs and deposited onto underlying substrates. The 50 nm thick Cr and 200 nm thick Au layers were prepared by dc sputtering at an argon pressure of 3×10^{-3} mbar and a dc current of 0.2 A. The Cr layer was used as an adhesive layer between Au and PET.[26] The substrate was repeatedly scanned under the arcing electrode to obtain a uniformly thick NiO film. It should be noted that the sparking process parameters were chosen based on the previous studies reported by our group,[27] which showed that higher sparking voltage could produce smaller average particle size. In particular, the maximum sparking voltage (3.0 kV) and sample sliding speed (1 cm min^{-1}) of the sparking machine were selected to obtain uniform sparked films with very fine nanometer-sized particles and high porosity. The mass of sparked NiO films was measured by high-precision microbalance with 6 digit resolution (M5P, Sartorius). The film mass was calculated by subtracting the substrate mass measured before NiO film deposition from the final mass measured afterwards. The average mass density of the film was determined from 8 samples (1×1 cm^2) to be 0.0375 mg cm^{-2}. The NiO electrodes would be characterized for electrochemical energy-storage performances without post-deposition annealing.

Material characterizations

The morphologies and nanostructures of NiO-NPs and NiO films were characterized using a field emission scanning electron microscope (FESEM, JEOL JSM-6335F) and transmission

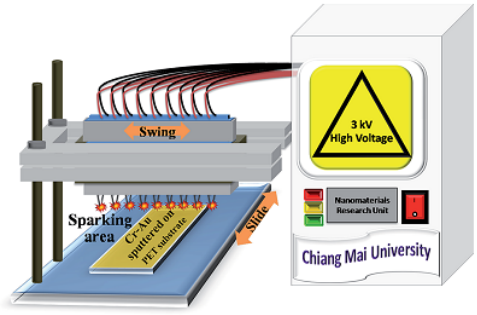

Fig. 1 Schematic illustration of the sparking system for fabrication of NiO films.

electron microscopy (TEM, JEOL JEM-2010). TEM samples were prepared by drop coating of NiO-NPs dispersion in acetone on a holey carbon/copper grid and TEM was operated at 200 kV and 108 mA. The selected area electron diffraction pattern (SAEDP) was also recorded to verify the crystal structure of NiO-NPs. The surface topography of NiO films was examined using an atomic force microscope (AFM, Nano Scope IIIa, Digital Instruments) equipped with a standard Si tip scanned over an area of 1×1 μm^2 in air at room temperature. The average surface roughness of the film was then calculated from AFM images of 4 different areas on a sample. In addition, the specific surface area and pore size distribution of the film were determined by Brunauer–Emmett–Teller (BET) and Barrett–Joyner–Halenda (BJH) nitrogen adsorption measurements (Autosorb 1 MP, Quantachrome). The samples were outgassed at 60 °C for 4 hour before the measurements. The band gap energy of sparked NiO film was determined by optical absorption spectroscopy using UV-vis spectrophotometer (Varian Cary 50, USA). The UV-vis sample was prepared by sparking of NiO-NPs on a glass substrate and UV-vis spectrum was measured in the wavelength range of ~300–800 nm. Besides, the oxidation state and chemical composition of the sparked NiO film were evaluated by X-ray photoelectron spectroscopy (XPS) using an AXIS Ultra DLD-X-ray photoelectron spectrometer and a monochromatic Al Kα X-ray excitation source.

Electrochemical measurement

The electrochemical energy-storage performances of the NiO films were evaluated at room temperature by CV and GCD measurements using an μ-Autolab Type III electrochemical work station (ECO-Chemie, Metrohm, Switzerland). The electrochemical measurements were conducted in a three-electrode configuration comprising a silver/silver chloride (Ag/AgCl) reference electrode, a platinum (Pt) wire counter electrode, the NiO working electrode and 1.0 M KOH electrolyte.

Results and discussion

Fig. 2 shows typical top-view and cross-sectional-view SEM images of a sparked NiO film. From the top-view image (Fig. 2(a)

and (b)), it can be seen that the film comprises very fine nanometer-sized particles loosely agglomerated into porous foam-like network. In addition, it contains a large number of pores with various sizes ranging from a few to hundreds nanometers. The cross-sectional view image (Fig. 2(c)) demonstrates that the NiO layer prepared by sparking method is a homogenous and regular film with high surface roughness. The average layer thickness is estimated to be ~2.6 ± 0.27 μm. The result confirms that a uniform film of loosely packed nanoparticles with microns in thickness can be effectively produced by the specially designed sparking system with electrode array and two-dimensional scanning.

The surface topography of the sparked NiO film was examined and compared with that of Cr–Au on PET substrate as illustrated in Fig. 3. It is seen that the NiO sparked film displays a bumpy surface comprising agglomerated secondary nanoparticles with diameters of less than 30 nm (Fig. 3(c) and (d)) while the substrate is much smoother with very shallow nanoprotrusions (Fig. 3(a) and (b)). The result is in agreement with the SEM observations in the top area of the porous foam network (Fig. 2(b)). The root-mean-square (RMS) surface roughness of the substrate and NiO sparked film are determined from the AFM data to be 4.4 ± 0.4 and 40.2 ± 3.6 nm, respectively. Thus, the RMS roughness of NiO sparked film is almost 10-fold as high as that of substrate. The high RMS roughness value of the film implies a large effective surface area and high rate of the electrochemical reaction.[28]

Fig. 4(a) displays a typical TEM image of NiO-NPs. It shows fine nanoparticles with uniform diameters randomly scattered on the surface. The corresponding HR-TEM image in Fig. 4(b) reveals that the nanoparticles are mostly spheroidal with varying diameters in the range of 3.0–6.0 nm. The results indicate that the sparking technique produces homogeneous nanoparticles with narrow particle size distribution. In addition, lattice fringes can be observed on some nanoparticles with

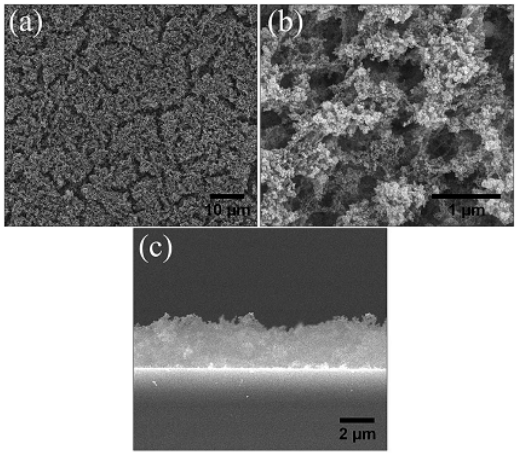

Fig. 2 The SEM images of the sparked NiO film: top-view at (a) low and (b) high magnifications and (c) cross-sectional-view.

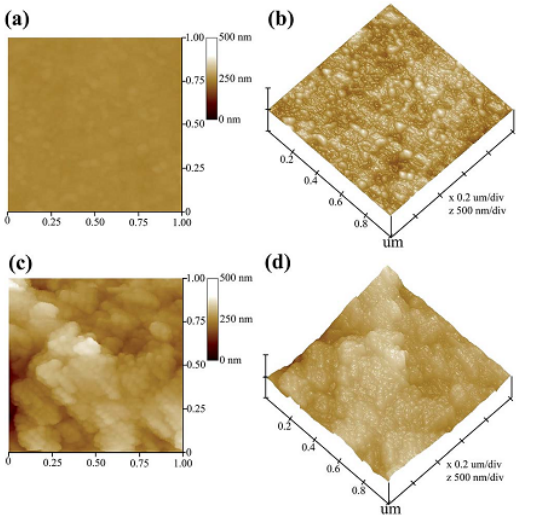

Fig. 3 (a) 2D, (b) 3D AFM topographic images of Cr–Au on PET substrate, (c) 2D and (d) 3D AFM topographic images of NiO sparked surfaces.

the inter planar distance of ~0.21 nm, which is corresponding to the *d*-spacing on (200) of cubic NiO.[29,30] The corresponding SAED pattern of NiO-NPs is shown in Fig. 4(c). It demonstrates ring diffraction patterns, identifying that the NiO particles have a polycrystalline structure. From indexing the diffraction pattern, the four main diffraction rings are found to closely match with the (111), (200), (220), and (311) planes of the cubic NiO phase (JCPDS 78-0429).[13] Thus, as-produced sparked powders are confirmed to be NiO nanoparticles with polycrystalline structure. Fig. 4(d) illustrates a typical EDS spectrum of the NiO-NPs on a carbon/copper TEM grid. It confirms all expected elements, including nickel (Ni), oxygen (O), copper (Cu) and carbon (C) of the nanoparticles and TEM grid. By excluding the elements from the grid, the atomic percentages of O and Ni are determined to be 47.6% and 52.4%, respectively. The composition is close to the ideal stoichiometric NiO.

Fig. 5 displays the N_2 adsorption–desorption isotherm of sparked NiO film. It can be seen that the film shows type VI pattern according to IUPAC classification,[31,32] corresponding to a stepwise multilayer adsorption process, which occurs due to a multimodal pore distribution. The estimated BET surface area from the adsorption data is ~16 $m^2 g^{-1}$, which is considered a high value for a thin film structure. The calculated BJH pore size distribution of the NiO film (inset of Fig. 5) demonstrates two maximum pore sizes at ~2.8 and ~10.4 nm, indicating the mesoporous structure. The high film porosity will provide an efficient transport pathway for ions to the interior of the sample, which is beneficial for electron transfer and adsorption, leading to a high charge capacity.

The GIXRD pattern of as-deposited NiO films on Au/Cr coated PET substrates is shown in Fig. 6(a). It is seen that the diffraction peaks can match well with the polycrystalline cubic

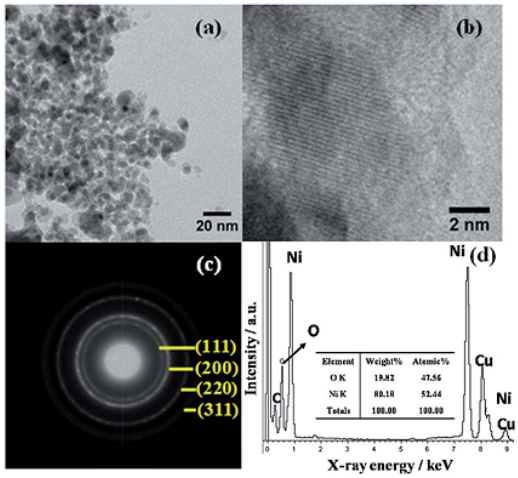

Fig. 4 (a) TEM image, (b) HR-TEM image, (c) SAED pattern and (d) EDX spectrum of sparked NiO-NPs.

NiO (JCPDS: 78-0429) and gold (JCPDS: 04-0784). For NiO, the diffraction on (111) plane is only clearly visible white diffractions on (200) and (220) are very weak and almost the same as background noise. The result is due to the fact that the GIXRD technique is not very sensitive to plane perpendicular to the film surface. Nevertheless, this method allows a significant reduction of diffraction from the Au film on PET substrate. It can also be noticed that there is a significant background slope at low diffraction angles due to the effect of amorphous PET substrate. In addition, it is observed that the NiO peaks appear to be quite narrow, implying quite large crystallite size of NiO nanoparticles in the film, which is in contrast to the observed nanoparticle size determined by TEM of 3–6 nm. The paradox could be due to the fact that diffraction signal of NiO is not much larger compared with that background noise so that the peak shape and related crystallite size are highly uncertain.

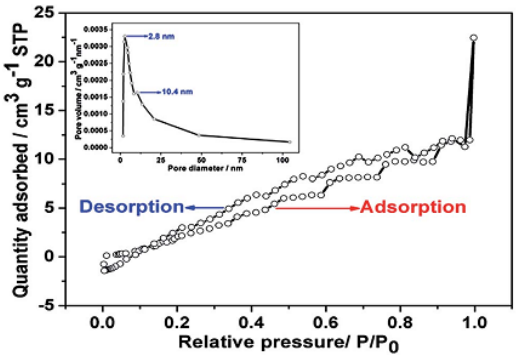

Fig. 5 Nitrogen adsorption and desorption isotherms of NiO film (inset: corresponding BJH pore size distribution).

Thus, GIXRD only allows the confirmation of NiO phase in the film while the actual crystallite size of NiO nanoparticles in the film cannot yet be determined but it can be implied that the value should be smaller than the size of TEM primary particles.

Fig. 6(b) illustrates a typical UV-vis spectrum of sparked NiO-NPs on glass substrate. It is seen that NiO-NPs exhibit strong absorption in the near-UV region, which can mainly be attributed to the band gap absorption.[33] The value of the band gap (E_g) can be calculated based on the fundamental absorption equation, which is given by:[34]

$$\alpha h\nu^n = (h\nu - E_g) \quad (1)$$

where α is the absorption coefficient, E_g is the energy band gap, $h\nu$ is photon energy, A is a constant relative to the materials and n is a characteristic number, 1/2 and 2 for indirect and direct band gap transitions, respectively. For NiO, $n = 2$ since it is a direct band gap semiconductor. The inset graph presents the plots of $(\alpha h\nu)^2$ as a function of $h\nu$. It is seen that the plot (black curve) is linear only in the high energy region (>3.6 eV) where fundamental band gap absorption occurs. The absorption at lower energy comes from other process such as absorption *via* defect states and thus does not conform to eqn (1). E_g of NiO-NPs is estimated to be around 3.47 eV by extrapolation of the linear region to the energy intercept (blue line). The value is in accordance with the value of NiO nanostructures in literature[35,36] and thus confirms the formation of NiO nanoparticles.

The surface compositions and chemical states of sparks NiO are further confirmed by using XPS. Fig. 7(a) shows the Ni 2p core levels of sparked NiO-NPs. The core levels, Ni $2p_{3/2}$ and Ni $2p_{1/2}$,

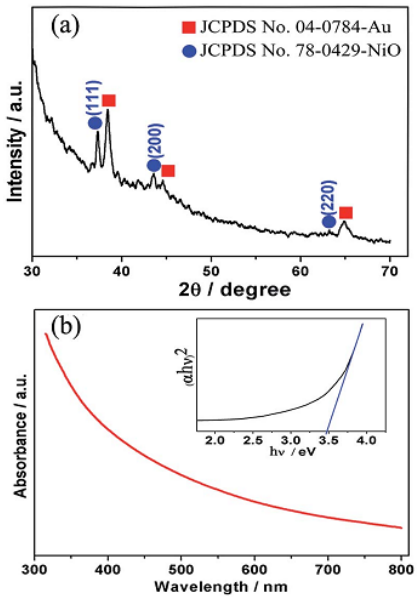

Fig. 6 (a) GIXRD pattern of sparked NiO film on Au/Cr coated PET substrate and (b) UV-vis spectrum (inset: plot of $(\alpha h\nu)^2$ *vs.* $h\nu$).

can be deconvoluted in to four doublet pairs at ~853.8 : 871.4, ~854.9 : 872.5, ~855.9 : 873.4 and ~857.2 : 874.7 eV, respectively. These doublet peaks may be assigned to Ni^{2+} of NiO, Ni^{2+} of $Ni(OH)_2$, Ni^{3+} of Ni_2O_3 and Ni^{3+} of NiOOH, respectively.[37–39] For the oxygen element (Fig. 7(b)), the O 1s core level spectrum can be similarly decomposed into four components located at ~529.3, ~530.9, ~532.0 and ~533.4 eV, respectively. The peak at 529.3 corresponds to the lattice oxygen of NiO while the ones at ~530.9, 532 and 533.4 eV can be assigned to adsorbed oxygen species, adsorbed OH– group due to humidity[12,40,41] and adsorbed –C–O– groups due to hydrocarbon impurities.[42] The results indicate that NiO-NPs formed by sparking method are complex nickel oxide.

The electrochemical characteristics of the sparked NiO film studied using CV and GCD are illustrated in Fig. 8. Fig. 8(a) shows a comparison of the CV curves in the potential window of 0 to 0.45 V (*vs.* Ag/AgCl) of the Cr–Au electrode on PET substrate with and without the sparked NiO films. It is evident that only NiO films exhibits high and sharp redox peaks, indicating its highly effective faradaic nature.[43] In contrast, the Cr–Au electrode on the PET substrate gives very low signal current and negligible peak. Thus, the NiO film will contribute almost all of charge storage capacity from the structure. The anodic and cathodic peaks at ~0.41 and ~0.32 V can be attributed to the redox reactions between NiO film and KOH electrolyte, in which NiOOH is oxidized to NiO and NiO is reduced to NiOOH, respectively. The reversible reaction is given by[40]

$$NiO + OH^- \leftrightarrow NiOOH + e^- \quad (2)$$

According to the XPS data, $Ni(OH)_2$ is also formed at the electrode surface. Thus, $Ni(OH)_2$ may also be reversibly converted to NiOOH according the redox reaction:[44,45]

$$Ni(OH)_2 + OH^- \leftrightarrow NiOOH + H_2O + e^- \quad (3)$$

However, the contribution of the reaction (3) to the redox peaks in CV should be relatively small since the fraction of $Ni(OH)_2$ found from the XPS data is considerably smaller than that of NiO.

Fig. 8(b) illustrates the CV profiles of the NiO film at different scan rates. It is seen that the CV peak current density increases monotonically with increasing scan rate, suggesting a good rate capability of the NiO films. In addition, the redox peak potential also increases accordingly with increasing scan rate. Fig. 8(c) shows the plot of the oxidation peak current *vs.* square root of scan rate. It is evident that the oxidation peak current is linearly proportional to the square root of scan rate, indicating that the redox reaction at NiO electrode is diffusion limited.[46] The characteristic is different from a typical capacitive behavior, in which peak current is proportional to the scan rate.

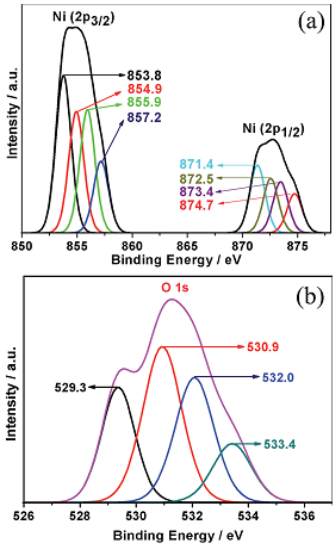

Fig. 7 (a) Ni 2p and (b) O 1s XPS spectra of sparked NiO film.

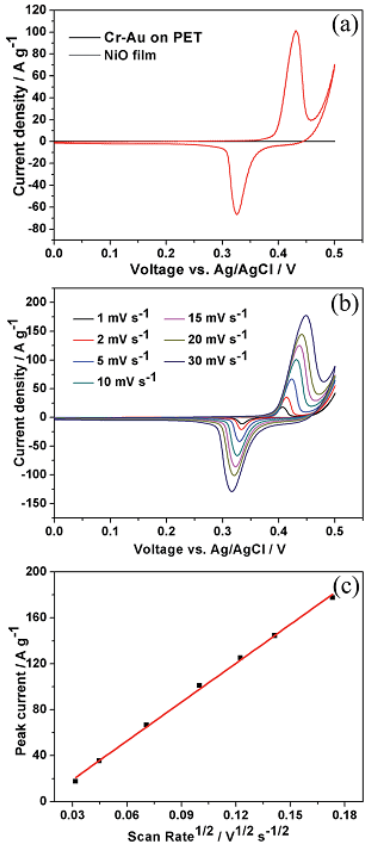

Fig. 8 (a) CV curve of the Cr–Au on PET substrate *vs.* sparked NiO film at a scan rate of 10 mV s^{-1}, (b) CV graph of NiO film at different scan rates and (c) oxidation peak current *vs.* square root of scan rate of sparked NiO film.

The energy-storage characteristic of NiO electrode is then evaluated by GCD technique. Fig. 9(a) and (b) displays GCD curves of NiO films at low and high ranges of discharge current density, respectively. It can be seen that all discharge curves consists of three regions with initial short fast discharge (0.45–0.4 V) followed by a long and slow discharge region (0.4–0.3 V) and final rapid discharge section (0.3–0 V), which is consistent with a typical characteristic of battery-like energy-storage device and in accordance with the faradaic CV behavior. The long discharge region corresponds to the potential at which redox peaks occur in the CV curve when the accumulated charges from redox reactions are released. Due to its battery-like characteristics, the performance of the sparked NiO electrode should be expressed in term of specific charge capacity (or in short specific capacity), which can be estimated from the GCD profile according to the defining equation:

$$\text{Specific charge capacity} = \frac{It}{m} \quad (4)$$

where I = discharge current, t = discharge time and m = mass of electrode material. From calculation, the sparked NiO electrode has the specific capacity values of 402.75, 368.55, 336.6, 308.7, 284.85, 275.85, 263.25 and 260.1 C g^{-1} at 1, 2, 4, 8, 16, 20, 28 and 40 A g^{-1}, respectively. The specific charge capacity is plotted as a function of current density as displayed in Fig. 9(c). It is evident that the specific capacity rapidly decreases as the current density increases from 1 to 8 A g^{-1} but then becomes very slow decreasing as the current density increases further from 8 to 40 A g^{-1}.

Moreover, the cycling performances of sparked NiO films at 40 A g^{-1} is demonstrated in Fig. 9(d) and (e). It can be seen that NiO electrode shows highly repeatable charging/discharging profile in the first 10 cycles (Fig. 9(d)). Furthermore, it has a good cycling ability with a good specific capacity retention of 88% for 1000 cycles of operation at the highest current density of 40 A g^{-1} (Fig. 9(e)). It is seen that the loss of capacity occurs mostly during first 300 cycles and the loss becomes much less as the number of cycles increases further up to 1000. The initial loss of capacity may be due to the agglomeration of the NiO particles[13,47] or structural change of NiO nanoparticles. This problem may be alleviated by appropriate post-deposition annealing of NiO film on the Au/PET substrate. Nevertheless, the sparked NiO film can maintain 88% of initial capacity up to 1000 cycles, which is still comparable with some other reports from porous NiO on Ni foam.[13]

In most reports on NiO-based electrochemical energy-storage devices, the performances were reported in term of specific capacitance instead of specific capacity due to the misconception of psuedocapacitor for nickel or cobalt oxide and hydroxide.[48] To compare the results with other reports, the average specific capacitance is converted from the specific capacity by dividing with the potential window used in this study of 0.45 V. The average specific capacitance values of sparked NiO electrode are calculated to be 895, 819, 748, 686, 633, 613, 585 and 578 F g^{-1} (or 33.6, 30.7, 29.1, 28.0, 27.1, 25.7, 25.0, 24.4, 23.7, 23.4, 23.0, 22.0 and 21.7 mF cm^{-2}) at 1, 2, 4, 8, 16, 20, 28 and 40 A g^{-1}, respectively. The values are comparable

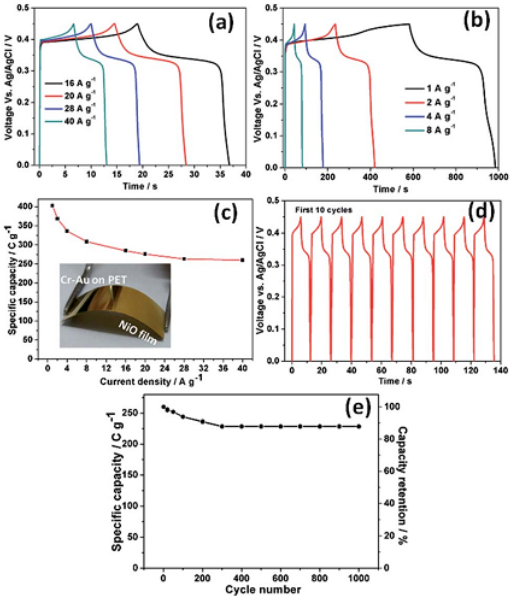

Fig. 9 (a–b) GCD data of NiO films at low and high ranges of discharge current density, (c) specific capacity curves at a variety of current densities (inset: photograph of bent electrode before testing), (d) GCD profiles of repeated 10 cycles at 40 A g^{-1} and (e) cycling performance of sparked NiO films at 40 A g^{-1}.

with some NiO-based devices, NiO nanoflowers, nanoslices and nanoparticles,[12] NiO flake-like and hierarchical porous ball-like,[49] porous thin film NiO nanowires,[50] mesoporous NiO nanoflake arrays[51] and NiO flower-like microspheres,[47] which report the specific capacitance in the range of 500–2000 F g^{-1} or 1–50 mF cm^{-2} at similar current densities. It should be noted that some work reported very high specific capacitance value but with narrower potential window or lower current density. Moreover, a preliminary mechanical durability test was performed. The electrochemical characteristics and specific capacity of sparked NiO film were not changed considerably after a typical rolling process. In addition, no physical delamination or damage of sparked NiO film was observed. Thus, the sparked NiO film could have sufficient mechanical stability for capacitor fabrication process.

The excellent electrochemical energy-storage performances of sparks NiO film may be attributed to large specific surface area of NiO NPs for redox reactions and charge storage. In addition, the porous structure of NiO films produced by sparking process assists the transportation of ions/electrons between electrode and electrolyte and reduce ion transfer resistance to the electrodes, which could result in a low effective series resistance.[22] The sparking technique can produce more porous structure compared with several other chemical methods since no binder is included, leading to the fully accessible surface area of NiO-NPs for electrochemical reaction. Thus, the sparked NiO film is considered to be an attractive

choice for electrochemical energy-storage applications due to low cost, simplicity and high charge capacity. Although the results achieved with the present sparking process parameters are considered decent, some parameters including scanning speed and the number of scanning cycles may be further optimized for optimal structure and electrochemical energy storage performances. The further optimization is under way and the results may be reported elsewhere.

Conclusions

In conclusion, NiO films were successfully fabricated by a sparking method and characterized for electrochemical energy-storage applications. The sparked NiO films exhibited excellent electrochemical energy storage performances with a high specific charge capacity of 402.75 C g^{-1} at a discharge current of 1 A g^{-1} and 88% capacity retention after 1000 cycles at a high discharge current of 40 A g^{-1}. The remarkable specific charge capacity could be attributed to the high electroactive surface area of highly porous films containing NiO nanoparticles. The key advantages of this technique include its convenient, low-temperature operation, and the low-cost system. Thus, the sparking method holds a promise as a practical and effective preparation technique of highly porous metal oxide films suitable for energy-storage applications.

Acknowledgements

The authors gratefully acknowledge the financial support by Thailand Graduate Institute of Science and Technology (TGIST), the Materials Science Research Center, Department of Physics and Materials Science, Faculty of Science, Chiang Mai University and the Graduate School, Chiang Mai University. Also, we would like to thank National Electronics and Computer Technology Center (NECTEC), Pathumthani, Thailand and Research Laboratory for Analytical Instrument and Electrochemistry Innovation, Faculty of Science, Chiang Mai University for electrochemical test. Moreover, the authors would like to acknowledge Mrs B. Kuntalue, Mr M. Kongtungmon T. Sakorn and E. Kuntarak for helping with TEM, SEM operation and AFM. In addition, the authors would like to thank Dr G. S. Roberts for language improvement.

Notes and references

1 B. T. Raut, S. G. Pawar, M. A. Chougule, S. Sen and V. B. Patil, *J. Alloys Compd.*, 2011, **509**, 9065–9070.
2 S. Pereira, A. Gonçalves, N. Correia, J. Pinto, L. Pereira, R. Martins and E. Fortunato, *Sol. Energy Mater. Sol. Cells*, 2014, **120**, 109–115.
3 H. Dalvand, G. Reza Khayati, E. Darezereshki and A. Irannejad, *Mater. Lett.*, 2014, **130**, 54–56.
4 G. Özkan and E. Özçelik, *J. Power Sources*, 2005, **140**, 28–33.
5 C. J. Hung, P. Lin and T. Y. Tseng, *J. Power Sources*, 2014, **259**, 145–153.
6 K. M. Kim, J. H. Nam, Y.-G. Lee, W. I. Cho and J. M. Ko, *Curr. Appl. Phys.*, 2013, **13**, 1702–1706.
7 J. Zhu, L. Cao, Y. Wu, Y. Gong, Z. Liu, H. E. Hoster, Y. Zhang, S. Zhang, S. Yang, Q. Yan, P. M. Ajayan and R. Vajtai, *Nano Lett.*, 2013, **13**, 5408–5413.
8 Q. Wang, L. Jiao, H. Du, Y. Wang and H. Yuan, *J. Power Sources*, 2014, **245**, 101–106.
9 R. S. Kalubarme, M.-S. Cho, K.-S. Yun, T.-S. Kim and C.-J. Park, *Nanotechnology*, 2011, **22**, 395402.
10 A. I. Inamdar, Y. Kim, S. M. Pawar, J. H. Kim, H. Im and H. Kim, *J. Power Sources*, 2011, **196**, 2393–2397.
11 A. Jena, N. Munichandraiah and S. A. Shivashankar, *J. Power Sources*, 2013, **237**, 156–166.
12 S.-I. Kim, J.-S. Lee, H.-J. Ahn, H.-K. Song and J.-H. Jang, *ACS Appl. Mater. Interfaces*, 2013, **5**, 1596–1603.
13 H. Wang, H. Yi, X. Chen and X. Wang, *Electrochim. Acta*, 2013, **105**, 353–361.
14 Y. Jiang, D. Chen, J. Song, Z. Jiao, Q. Ma, H. Zhang, L. Cheng, B. Zhao and Y. Chu, *Electrochim. Acta*, 2013, **91**, 173–178.
15 X.-h. Xia, J.-p. Tu, X.-l. Wang, C.-d. Gu and X.-b. Zhao, *J. Mater. Chem.*, 2011, **21**, 671–679.
16 M.-S. Wu, C.-Y. Huang and K.-H. Lin, *J. Power Sources*, 2009, **186**, 557–564.
17 M.-S. Wu, Y.-A. Huang, C.-H. Yang and J.-J. Jow, *Int. J. Hydrogen Energy*, 2007, **32**, 4153–4159.
18 M.-S. Wu, C.-H. Yang and M.-J. Wang, *Electrochim. Acta*, 2008, **54**, 155–161.
19 M. M. Rahman, S.-L. Chou, C. Zhong, J.-Z. Wang, D. Wexler and H.-K. Liu, *Solid State Ionics*, 2010, **180**, 1646–1651.
20 X.-M. Liu, X.-G. Zhang and S.-Y. Fu, *Mater. Res. Bull.*, 2006, **41**, 620–627.
21 I. Porqueras and E. Bertran, *Thin Solid Films*, 2001, **398–399**, 41–44.
22 H. Wang, Y. Wang and X. Wang, *Electrochem. Commun.*, 2012, **18**, 92–95.
23 W. Thongsuwan, T. Kumpika and P. Singjai, *Curr. Appl. Phys.*, 2008, **8**, 563–568.
24 K. Hongsith, N. Hongsith, D. Wongratanaphisan, A. Gardchareon, S. Phadungdhitidhada, P. Singjai and S. Choopun, *Thin Solid Films*, 2013, **539**, 260–266.
25 K. Inyawilert, A. Wisitsora-at, A. Tuantranont, P. Singjai, S. Phanichphant and C. Liewhiran, *Sens. Actuators, B*, 2014, **192**, 745–754.
26 I. Nam, S. Park, G.-P. Kim, J. Park and J. Yi, *Chem. Sci.*, 2013, **4**, 1663–1667.
27 T. Kumpika, W. Thongsuwan and P. Singjai, *Surf. Interface Anal.*, 2007, **39**, 58–63.
28 S. Cho, K.-H. Shin and J. Jang, *ACS Appl. Mater. Interfaces*, 2013, **5**, 9186–9193.
29 H. Long, T. Shi, H. Hu, S. Jiang, S. Xi and Z. Tang, *Sci. Rep.*, 2014, **4**, DOI: 10.1038/srep07413.
30 A. Kumar, A. Saxena, A. De, R. Shankar and S. Mozumdar, *Adv. Nat. Sci.: Nanosci. Nanotechnol.*, 2013, **4**, 025009.
31 V. Kruefu, A. Wisitsoraat and S. Phanichphant, *J. Nanomater.*, 2015, **2015**, 8.
32 J. H. de Boer, B. C. Lippens, B. G. Linsen, J. C. P. Broekhoff, A. van den Heuvel and T. J. Osinga, *J. Colloid Interface Sci.*, 1966, **21**, 405–414.

33 S. Nandy, S. Goswami and K. K. Chattopadhyay, *Appl. Surf. Sci.*, 2010, **256**, 3142–3147.
34 M. Salavati-Niasari, N. Mir and F. Davar, *J. Alloys Compd.*, 2010, **493**, 163–168.
35 V. Patil, S. Pawar, M. Choug, P. Godse, R. Sakhare, S. i. Sen and P. Joshi, *J. Surf. Eng. Mater. Adv. Technol.*, 2011, **1**, 35–41.
36 L.-P. Zhu, G.-H. Liao, Y. Yang, H.-M. Xiao, J.-F. Wang and S.-Y. Fu, *Nanoscale Res. Lett.*, 2009, **4**, 550–557.
37 J.-Z. Huang, Z. Xu, H.-L. Li, G.-H. Kang and W.-J. Wang, *Trans. Nonferrous Met. Soc. China*, 2006, **16**, 1301–1306.
38 Y. Li and Y. He, *RSC Adv.*, 2014, **4**, 16879–16884.
39 M. V. Bykova, D. Y. Ermakov, V. V. Kaichev, O. A. Bulavchenko, A. A. Saraev, M. Y. Lebedev and V. A. Yakovlev, *Appl. Catal., B*, 2012, **113–114**, 296–307.
40 J. B. Wu, R. Q. Guo, X. H. Huang and Y. Lin, *J. Power Sources*, 2013, **243**, 317–322.
41 A. Fihri, R. Sougrat, R. B. Rakhi, R. Rahal, D. Cha, M. N. Hedhili, M. Bouhrara, H. N. Alshareef and V. Polshettiwar, *ChemSusChem*, 2012, **5**, 1241–1248.
42 X. Feng, N. Dementev, W. Feng, R. Vidic and E. Borguet, *Carbon*, 2006, **44**, 1203–1209.
43 G. X. Pan, X. H. Xia, F. Cao, P. S. Tang and H. F. Chen, *Electrochem. Commun.*, 2013, **34**, 146–149.
44 R. A. Huggins, *Advanced Batteries: Materials Science Aspects*, Springer Science & Business Media, 2008.
45 R. Mohd Syafiq Hamdan and M. R. Othman, *Int. J. Electrochem. Sci.*, 2013, **8**, 4747–4760.
46 B. Vidhyadharan, N. K. M. Zain, I. I. Misnon, R. A. Aziz, J. Ismail, M. M. Yusoff and R. Jose, *J. Alloys Compd.*, 2014, **610**, 143–150.
47 D. Du, Z. Hu, Y. Liu, Y. Deng and J. Liu, *J. Alloys Compd.*, 2014, **589**, 82–87.
48 T. Brousse, D. Bélanger and J. W. Long, *J. Electrochem. Soc.*, 2015, **162**, A5185–A5189.
49 S. K. Meher, P. Justin and G. Ranga Rao, *ACS Appl. Mater. Interfaces*, 2011, **3**, 2063–2073.
50 A. Paravannoor, R. Ranjusha, A. M. Asha, R. Vani, S. Kalluri, K. R. V. Subramanian, N. Sivakumar, T. N. Kim, S. V. Nair and A. Balakrishnan, *Chem. Eng. J.*, 2013, **220**, 360–366.
51 X. Yan, X. Tong, J. Wang, C. Gong, M. Zhang and L. Liang, *J. Alloys Compd.*, 2014, **593**, 184–189.

APPENDIX B

Yaowamarn Chuminjak, Suphaporn Daothong, Aekapong Kuntarug, Ditsayut Phokharatkul, Mati Horprathum, Anurat Wisitsoraat, Adisorn Tuantranont, Jaroon Jakmunee and Pisith Singjai, “ High-performance Electrochemical Energy Storage Electrodes Based on Nickel Oxide-coated Nickel Foam Prepared by Sparking Method”, 238, 2017, Pages 298-30.

Electrochimica Acta 238 (2017) 298–309

Contents lists available at ScienceDirect

Electrochimica Acta

journal homepage: www.elsevier.com/locate/electacta

High-performance Electrochemical Energy Storage Electrodes Based on Nickel Oxide-coated Nickel Foam Prepared by Sparking Method

Yaowamarn Chuminjak[a,b], Suphaporn Daothong[c], Aekapong Kuntarug[a], Ditsayut Phokharatkul[d], Mati Horprathum[d], Anurat Wisitsoraat[d], Adisorn Tuantranont[d], Jaroon Jakmunee[e], Pisith Singjai[a,f,*]

[a] Department of Physics and Materials Science, Faculty of Science, Chiang Mai University, Chiang Mai, 50200, Thailand
[b] Graduate School Chiang Mai University, Chiang Mai, 50200, Thailand
[c] Program in Materials Science, Faculty of Science, Maejo University, Chiang Mai, 50290, Thailand
[d] Nanoelectronics and MEMS Laboratory, National Electronics and Computer Technology Center, National Science and Technology Development Agency, Klong Luang, Pathumthani, 12120, Thailand
[e] Research Laboratory for Analytical Instrument and Electrochemistry Innovation, Faculty of Science, Chiang Mai University, Chiang Mai 50200, Thailand
[f] Materials Science Research Center, Faculty of Science, Chiang Mai University, Chiang Mai 50200, Thailand

ARTICLE INFO

Article history:
Received 27 January 2017
Received in revised form 22 March 2017
Accepted 26 March 2017
Available online 7 April 2017

Keywords:
NiO nanoparticles
Sparking method
Ni foam
Electrochemical energy storage

ABSTRACT

In this work, high-performance electrochemical energy storage electrodes were developed based on nickel oxide (NiO)-coated nickel (Ni) foams prepared by a sparking method. NiO nanoparticles deposited on Ni foams with varying sparking times from 45 to 180 min were structurally characterized by scanning electron microscopy, energy dispersive X-ray spectroscopy, transmission electron microscopy, X-ray photoelectron spectroscopy and Raman spectroscopy. In addition, the electrochemical energy storage characteristics of the electrodes were evaluated by cyclic voltammetry, galvanostatic charge-discharge and electrochemical impedance spectroscopy. It was found that NiO nanoparticles sparked on Ni foam with a longer time would be agglomerated and formed a foam-like network with large pore sizes and a lower surface area, leading to inferior charge storage behaviors. The NiO/Ni foam electrode prepared with the shortest sparking of 45 min displayed high specific capacities of 920 C g^{-1} (1840 F g^{-1}) at 1 A g^{-1} and 699 (76% of 920) C g^{-1} at 20 A g^{-1} in a potential window of 0–0.5 V vs. Ag/AgCl as well as a good cycling performance with 96% capacity retention at 4 A g^{-1} after 1000 cycles and a low equivalent series resistance of 0.4 Ω. Therefore, NiO/Ni foam electrodes prepared by the sparking method are highly promising for high-capacity energy storage applications.

1. Introduction

Electrochemical energy storage devices have recently earned great attention due to increasing demand for use in power grid systems, electric vehicles, and portable electronic devices such as smartphones, tablets, laptops and cameras. Much research has thus been focusing on the development of high-performance electrochemical energy storage devices with high power/energy capacity, high charge/discharge rates, high charge/discharge efficiency, small size, light weight, long cycle life, low cost and environmental friendliness [1,2]. According to charge/discharge behaviors, electrochemical energy storage devices may be broadly categorized into two main groups, namely supercapacitor and battery-type charge storage [3,4]. Supercapacitor is a class of electrochemical devices that exhibit a linear dependence of the charge versus potential within a potential window and displays triangular-shape charge/discharge as well as rectangular-shape cyclic voltammetric (CV) curves. Its energy storage mechanism is primarily based on electric double-layer capacitors (EDLCs), which store energy through electrostatic adsorption/desorption of ions taking place at the interface between electrode and electrolyte [5,6]. Well-known EDLC materials are noble metals and carbonaceous materials such as activated carbon [7,8], carbon nanotubes [9,10], and graphene [11,12]. The other alternative mechanism for supercapacitor is pseudocapacitance, which implicates charge passage through the double layers like faradaic process but having a linear relationship between charge and potential due to thermodynamic reasons [13]. Pseudocapacitive

* Corresponding author.
E-mail address: pisith.s@cmu.ac.th (P. Singjai).

http://dx.doi.org/10.1016/j.electacta.2017.03.190
0013-4686/

materials include some metal oxides such as MnO_2 and RuO_2 as well as some conductive polymers such as polyaniline and polypyrrole [14–17].

In contrast, the battery-type devices show oxidation/reduction CV peaks and nonlinear charge/discharge characteristics. The mechanism of a battery-type device is purely faradaic involving redox reactions at the surfaces of active electrode material [4]. Some transition metal oxides (TMOs) and hydroxides including NiO [18], Co_3O_4 [19], V_2O_5 [20,21], MoO_3 [22], $Ni(OH)_2$ [23,24] and $Co(OH)_2$ [25,26] are recently reported as promising battery-type electrode materials. Among these, NiO is particularly attractive due to its high charge capacity, fast faradaic reactions, high stability, environmental harmlessness and low cost [27,28]. The electrochemical energy storage performances of a NiO electrode depend

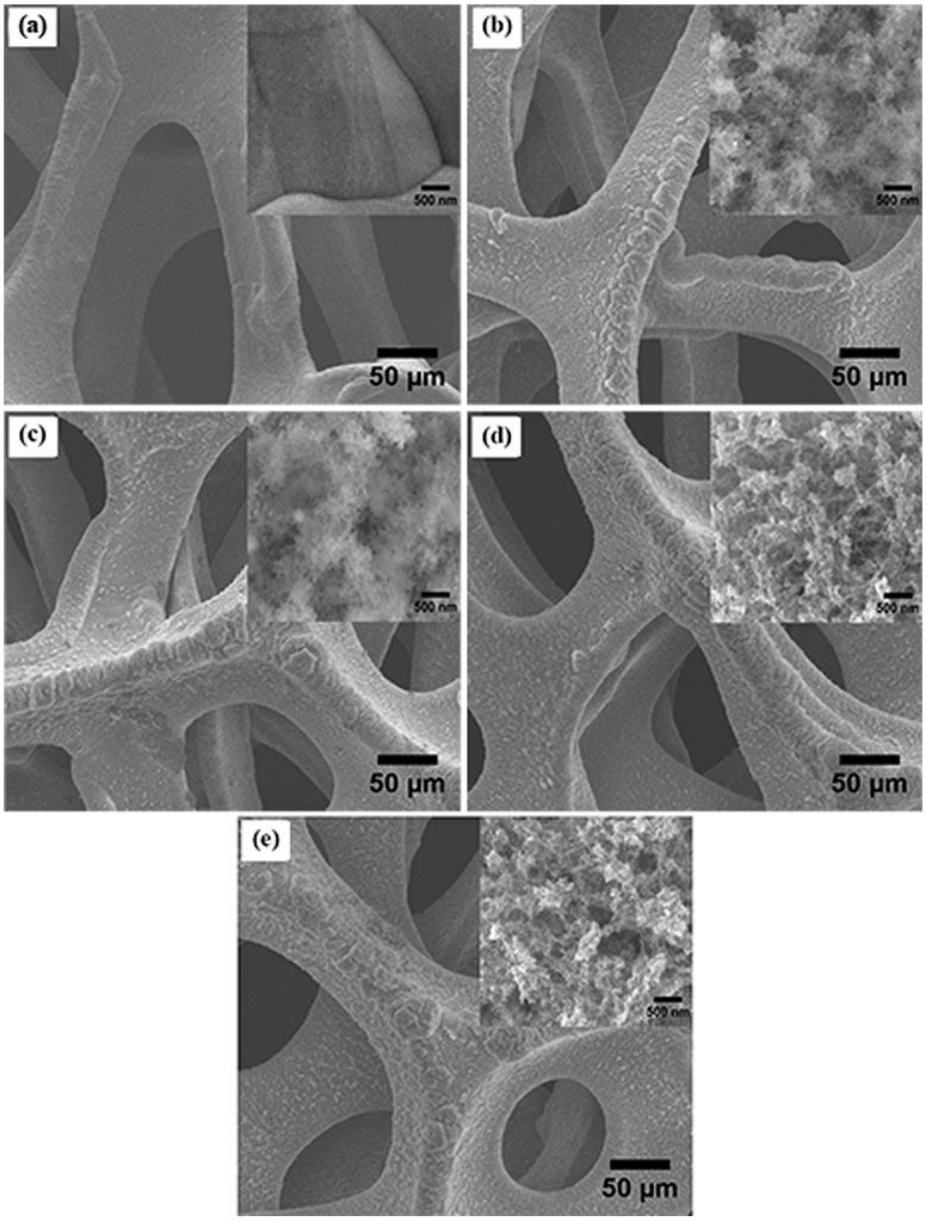

Fig. 1. SEM images of (a) Ni foam, (b) NiO-45 min, (c) NiO-90 min, (d) NiO-135 min and (e) NiO-180 min.

considerably on its production method and electrode structure since they directly affect electronic conductivity and specific surface area [29]. For instance, NiO thin films fabricated by a spray deposition process exhibited a specific capacity of ~162 C g^{-1} at 5 mV s^{-1} [30]. In addition, NiO thin films produced by a chemical precipitation technique displayed a good specific capacity of ~200.4 C g^{-1} at 20 mV s^{-1} [31]. Moreover, NiO nanoparticles synthesized via a hydrothermal method showed a high specific capacity of ~476.3 C g^{-1} at 1 A g^{-1} [32]. Similarly, NiO nanostructures with spherical sponge morphologies fabricated by another chemical precipitation process offered a decent specific capacity of ~505 C g^{-1} at 1 A g^{-1} [33]. Likewise, NiO nanoplatelets prepared using a microwave-assisted method demonstrated a superior specific capacity of 548 C g^{-1} at 1 A g^{-1} [34]. From these reported results, the energy storage performances of NiO-based electrode can be enhanced by the creation of nanostructures by an effective synthesis method. It is thus compelling to explore an alternative method for the preparation of NiO-based electrode in order to yield high-performance NiO-based energy storage devices.

Sparking is a relatively new method for production of TMO nanostructures including NiO [35], In_2O_3 [36], TiO_2 [37,38] and ZnO [39,40] nanoparticles due to its ability to produce highly porous nanostructured films with very small structural size, homogenous composition and well controlled film thickness in one step at low cost. It has been demonstrated to be promising for a variety of applications including electrochemical energy storage devices, gas sensors, photocatalysis, and double-layered photoelectrodes in dye-sensitized solar cells. Recently, it has been successfully employed to fabricate a porous NiO film on a flexible chromium/gold coated polyethylene terephthalate substrate that offers a promising specific capacity of 402.75 C g^{-1} at 1 A g^{-1} [35]. Nevertheless, its charge storage performances should be further improved by the use of a porous substrate with an optimized sparking condition. In this work, NiO nanostructures are coated on porous nickel foams by sparking with varying sparking times and their structures and electrochemical performances are systematically characterized for energy storage applications.

2. Experimental

2.1. Fabrication of NiO films

All analytical-grade chemicals (Sigma-Aldrich) including acetone, KOH and HCl were used without further purification. NiO films were deposited on Ni foam substrates based on the sparking procedure reported in our previous work [35]. In brief, Ni foam substrates were prepared by cutting a 1 mm-thick Ni foam sheet (110 pores per inch) into 1×2 cm^2 pieces, which were then cleaned in acetone under sonication for 20 min and dried by nitrogen gas. NiO was deposited by direct sparking from an array of 0.25 mm-diameter nickel wires (99.98%, Advent Research Material Ltd, Oxford, UK) at 3 kV and 10 mA onto Ni foam substrates at a fixed substrate-Ni wire spacing of 5 mm. The sparking time was varied from 45 to 180 min with an increment of 45 min. The samples were labeled with the sparking time as NiO-sparking time (45 min, 90 min, 135 min and 180 min). The sparking process was repeated on the other side of substrate in order to fully cover the surfaces of Ni foams with NiO. The mass of sparked NiO material was measured by a high-precision microbalance with 5 digit resolution (240A, Precisa). The film mass was calculated by subtracting the substrate mass measured before NiO film deposition from the final mass measured afterwards. The average mass densities of NiO sparked on Ni foams for 45, 90, 135 and 180 min were determined to be 0.15, 0.26, 0.38 and 0.53 mg cm^{-2}, respectively.

2.2. Structural Characterization

The structures and morphologies of NiO nanoparticles and NiO layers on Ni foams were examined using a field-emission scanning electron microscopy (FE-SEM, Hitachi model SU-8030) and transmission electron microscopy (TEM, JEOL model JEM-2010). The selected area electron diffraction (SAED) pattern was recorded to verify the crystal structure of NiO nanopowder. The corresponding elemental composition was determined by energy dispersive X-ray (EDX) spectroscopy. The chemical bonding of sparked NiO nanostructures on Ni foams were evaluated by Raman spectroscopy (RAMAN, Renishaw model Invia) using the 532 nm laser with 4.9 mW power. In addition, the oxidation state and surface chemical composition of NiO nanoparticles on Ni foams were assessed by X-ray photoelectron spectroscopy (XPS, AXIS Ultra DLD-X-ray photoelectron spectrometer) equipped with a monochromatic Al K_α X-ray source.

2.3. Electrochemical measurement

Cyclic voltammetric (CV), galvanostatic charge-discharge (GCD) and electrochemical impedance spectroscopic (EIS) measurements were conducted at room temperature using a computer-controlled potentiostat-galvanostat operated by Nova 1.10 software package (ECO-Chemie, Metrohm, PGSTAT302N). All electrochemical measurements were carried out with a three-electrode system in a 3 mol l^{-1} KOH electrolyte. A silver/silver chloride (Ag/AgCl), a platinum (Pt) wire and NiO/Ni foam electrode (1x1 cm^2) were used as the reference, counter and working electrodes, respectively. EIS data were recorded over the frequency range of 10 mHz - 100 kHz with an applied AC voltage of 5 mV and an open-circuit DC potential.

3. Results and discussion

3.1. Structural characteristics

Fig. 1 displays the surface morphologies of NiO nanostructures on Ni foams with different sparking times ranging from 45 to 180 min compared with that of a bare Ni foam. It is seen that the Ni foam has large pores whose dimensions are in the range of 100-300 μm and relatively thin lamellae whose widths are varying between 30 and 80 μm. The inset high-magnification image of a bare Ni foam shows a smooth polycrystalline surface having domain size of around few microns (Fig. 1 (a)). After NiO sparking for 45 min, the surface becomes porous and fluffy due to the presence of very fine nanometer-sized particles along with some small voids and cavities (Fig. 1 (b)). The particles are so small that their boundaries cannot be clearly resolved by SEM. When the sparking time increases to 90 min, it can be observed that particles begin to agglomerate into larger cluster leaving some deeper cavities (Fig. 1 (c)). At a longer sparking time of 135 min, nanoparticles clearly aggregate into a number of clusters with a few hundred nanometer in size that are loosely connected into a foam-like network having a number of pores with sizes ranging from a few to several hundreds of nanometers. With the longest sparking time of 180 min, the clusters grow in size and number while the cavities become relative small, suggesting the densification of particulate network at very long sparking time. From the observations, the morphology of sparked NiO structure on Ni foam depends considerably on the sparking time. Initially, nanoporous fluffy films of NiO nanoparticles are formed at a short sparking time (45 min) and NiO nanoparticles will be aggregated into larger clusters loosely connected in the form of foam-like microporous network as the sparking time increases. The surface area of NiO structures should be initially high and tend to reduce due to

increasing average cluster and pore sizes as the sparking time increases. The results are partly in accordance with the previous report of sparked In_2O_3 films on alumina substrates, which demonstrated a correlation between the morphologies of sparked films and the number of sparking cycles [36]. The observed effect may be explained based on the influence of sparking time on the temperature of arcing plasma. In the sparking process, arcing plasma generated through field ionization process will dissipate a part of its energy into heat, inducing elevated plasma and substrate temperatures, which will monotonically increase with increasing sparking time. The higher plasma temperature can affect the electric field and charge distributions of the plasma, leading to the redistribution of sparked NiO particles into nonuniform patterns, resulting in the formation of localized clusters at a long sparking time. In addition, the increase of underlying substrate temperature can accelerate the aggregation of primary particles into secondary particles or clusters [37].

The corresponding EDX spectra of NiO nanostructures on Ni foams are demonstrated in Fig. 2. It is evident that all samples contain all expected elements including Ni and O of Ni foam and sparked NiO film. For the bare Ni foam (Fig. 2 (a)), the small oxygen content of 10.86 at% is found and known to be attributed to the native oxide layer on Ni surface [41] With the presence of NiO layers (Fig. 2 (b)-(c)), the oxygen content increases rapidly from 31.66 to 49.12 at% as the sparking time increases from 45 to 90 min. The results confirm that the sparked Ni particles have been

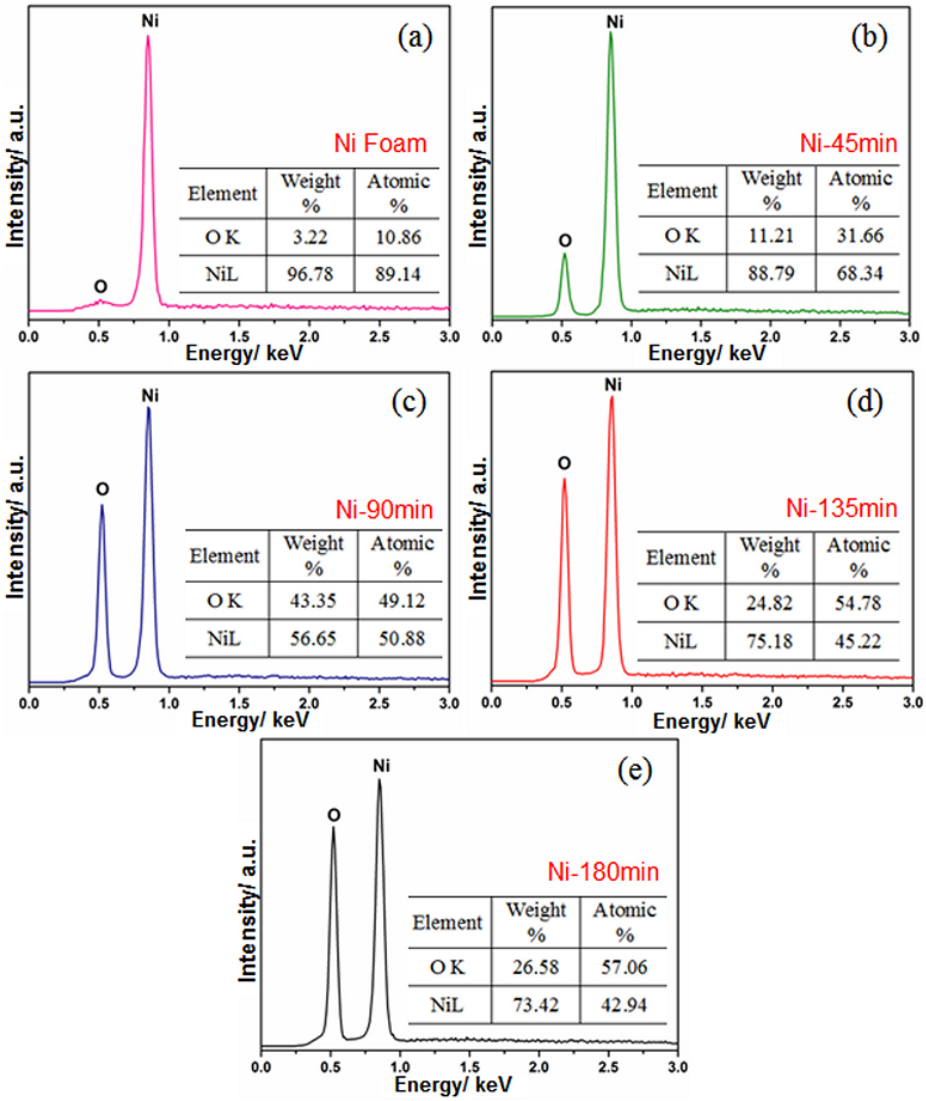

Fig. 2. The corresponding EDX spectra of (a) Ni foam, (b) NiO-45 min, (c) NiO-90 min (d) NiO-135 min, and (e) NiO-180 min.

oxidized in air during sparking at a high plasma temperature of >1000 °C [37]. The increasing O content can correlate with the increasing thickness of sparked NiO film since the EDX elemental information comes from both NiO layer and Ni foam substrate through the electron penetration depth of 2-3 μm at 20 kV. As the sparking time increases further from 90 to 180 min, the oxygen concentration increases only slightly from 49.12 to 57.06 at%, indicating that the film thicknesses are comparable with or larger than the electron penetration depth so that the EDX information already mainly arises from the sparked NiO layer. However, the oxygen content values tend to be higher than that of the stoichiometric NiO (50 at%). This could be due to inaccuracy of EDX measurement or the excess oxygen in the sparked NiO materials. The actual surface elemental composition of NiO nanostructures will be verified by XPS measurements.

Fig. 3 (a) and (b) illustrate the TEM images of NiO nanoparticles produced at sparking times of 45 and 180 min, respectively. It is seen that the sparked NiO nanoparticles are mostly spheroidal and occasionally ellipsoidal with sub-ten nanometer dimensions. In addition, some primary NiO nanoparticles aggregate into larger secondary particles or clusters. The diameters of primary NiO nanoparticles with sparking times of 45 and 180 min are estimated to be 4.3 ± 1.7 and 7.6 ± 2.5 nm, respectively. Thus, the sparking process can produce homogeneously small NiO nanoparticles and the particle size tends to increase with increasing sparking time. This effect may also be attributed to the influence of sparking time on substrate temperature. With increasing sparking time, the substrate temperature increases accordingly, leading to the rapid growth of sparked particles. The corresponding SAED patterns of both samples (insets) display diffraction rings, which can be indexed as (111), (200), (220) and (311) planes of a cubic NiO phase (JCPDS 78-0429), confirming that the observed nanoparticles are NiO with a polycrystalline structure [27].

Fig. 4 demonstrates Raman spectra of NiO nanostructures on Ni foam deposited with different sparking times. It shows that sparked NiO structures exhibit broad Raman peaks at around 402, 559, 735, 901, 1107, and 1594 cm^{-1}, which can be assigned to 1TO (1^{st} order transverse optical phonon), 1LO (1^{st} order longitudinal optical phonon), 2TO (2^{nd} order TO), TO + LO (1^{st} order superposition) and 2LO (2^{nd} order LO) vibration modes of the cubic NiO structure [42–45]. However, the two-magnon band (2 M) expected to appear in the range of 1400-1500 cm^{-1} are not found [45,46]. In addition, there is a shallow band at 1594 cm^{-1} corresponding to amorphous carbon phase [45], which is expected to arise from some carbon impurities. Moreover, it can be observed that the

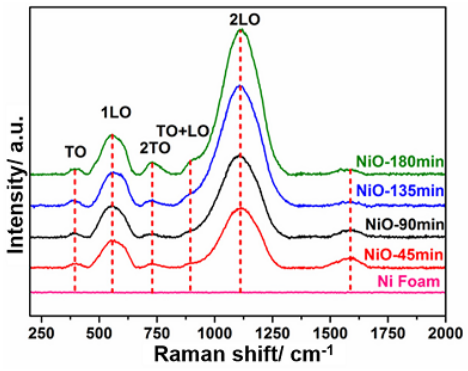

Fig. 4. Raman spectra of sparked NiO nanoparticles on Ni foams with different sparking times.

Raman peak intensities of NiO films tends to become more apparent, confirming the higher amount of NiO material with increasing sparking time.

Representative XPS spectra of NiO/Ni foams produced at the sparking times of 45 and 180 min are illustrated in Fig. 5. The survey-scan XPS spectra of NiO/Ni foams (Fig. 5 (a)) display the main XPS and Auger peaks of Ni, O and C, affirming the existence of NiO structure and some carbon contaminations. By omitting the content of carbon contamination, the surface elemental compositions of NiO-45 min and NiO-180 min reveal the oxygen contents of 62.2 and 59.3 at%, respectively. The values are considerably higher than that of the stoichiometric NiO (50 at%), suggesting the presence of nickel oxide with higher oxidation states (Ni_2O_3 or NiO_2) and/or nickel oxyhydroxide (NiOOH) on surface. For Ni element (Fig. 5 (b)), the Ni 2p doublet pair, Ni $2p_{3/2}$:Ni $2p_{1/2}$, of NiO-45 min can be deconvoluted by Gaussian fitting into three doublet pairs at the binding energies of 854.2:872.0, 855.6:873.5 and 856.9:874.9 eV while that of NiO-180 min can be decomposed into four doublet components at 853.8:871.4, 854.9:872.5, 855.9:873.4 and 857.2:874.7 eV, respectively. The energy separations (Ni $2p_{1/2}$-Ni $2p_{3/2}$) of the main Ni 2p doublet peaks (before deconvolution) for NiO-45 min and NiO-180 min are both equal to 17.9 eV in close agreement with most reports for NiO (17.8 eV) [47]. The peaks at 853.8–854.2, 854.9, 855.6–855.9 and 856.9–857.2 may be assigned to Ni^{2+} of NiO, mixed Ni^{2+}-Ni^{3+} of β-NiOOH, Ni^{2+} of $Ni(OH)_2$ and Ni^{3+} of α-NiOOH, respectively

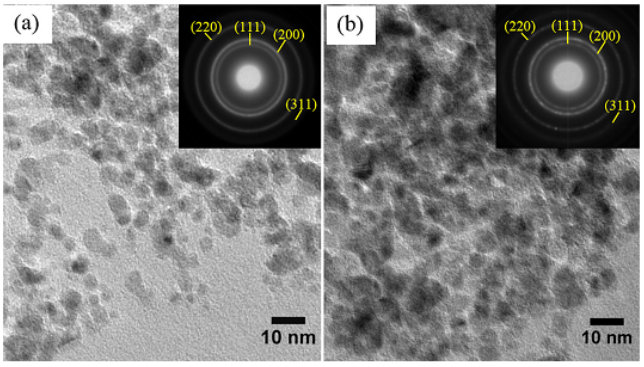

Fig. 3. TEM images and corresponding SAED patterns of NiO nanoparticles produced at sparking times of (a) 45 and (b) 180 min.

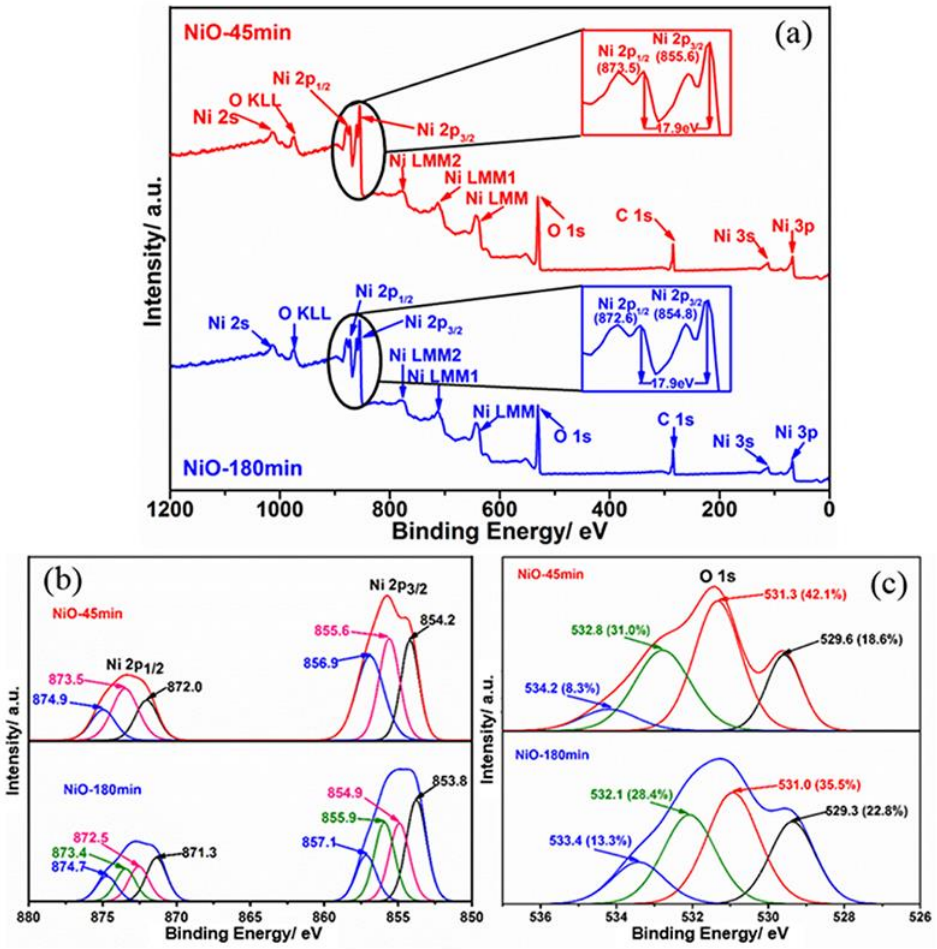

Fig. 5. XPS spectra of NiO nanoparticles on Ni foams produced at sparking times of 45 and 180 min: (a) survey scan, (b) Ni 2p and (c) O 1s.

[48,49]. Thus, sparked NiO structures prepared at 45 and 180 min have similar NiO/OH phase components but NiO-180 min contains an additional β-NiOOH phase. In addition, it can be seen from the relative peak areas that NiO-45 min comprises relatively high fraction of nickel hydroxide species.

In the case of oxygen (Fig. 5 (c)), the O 1s peak of NiO-45 min can be decomposed into four components centered at the binding energy of 529.6, 531.3, 532.8 and 534.2 eV while those of NiO-180 min are slightly shifted to 529.3, 531.0, 532.1 and 533.4 eV, respectively. They can be attributed to the lattice oxygen (O^{2-}) of NiO, chemisorbed hydroxide species (OH^-) [2,50], adsorbed oxyhydroxide species (OOH^-) group due to humidity [51] and loosely bound oxygen species at defect sites and carbonaceous impurities [52], respectively. Moreover, the contribution of OH^- (42.1%) and OOH^- (31.0%) for NiO-45 min are notably higher than those for NiO-180 min (35.5 and 28.4%) in accordance with the observed Ni species. Thus, the results indicate that the fraction of fully oxidized NiO in sparked NiO nanostructures tends to increase with increasing sparking time. This result should be due to increasing plasma and substrate temperatures, leading to the higher degree of Ni oxidation during sparking with increasing sparking time.

3.2. Electrochemical properties of NiO/Ni foam electrodes

The CV data of sparked NiO/Ni foam electrodes with different sparking times are demonstrated in Fig. 6. The CV curves of all NiO/Ni foam electrodes at various scan rates ranging from 5 to 50 mV s^{-1} (Fig. 6 (a-d)) display strong anodic and cathodic peaks, indicating that the charge capacities of these electrodes mainly arise from Faradaic redox reactions at the electrode surface and the sparked NiO on Ni foam is a battery-type electrochemical energy storage electrode [29]. The redox peaks may be attributed to two reversible redox reactions of $Ni(OH)_2$/NiOOH and NiO/NiOOH according to [53–56]:

$$Ni(OH)_{2+}\ OH^- \Leftrightarrow NiO(OH) + H_2O + e^- \quad (1)$$

$$NiO + OH^- \Leftrightarrow NiO(OH) + e^- \quad (2)$$

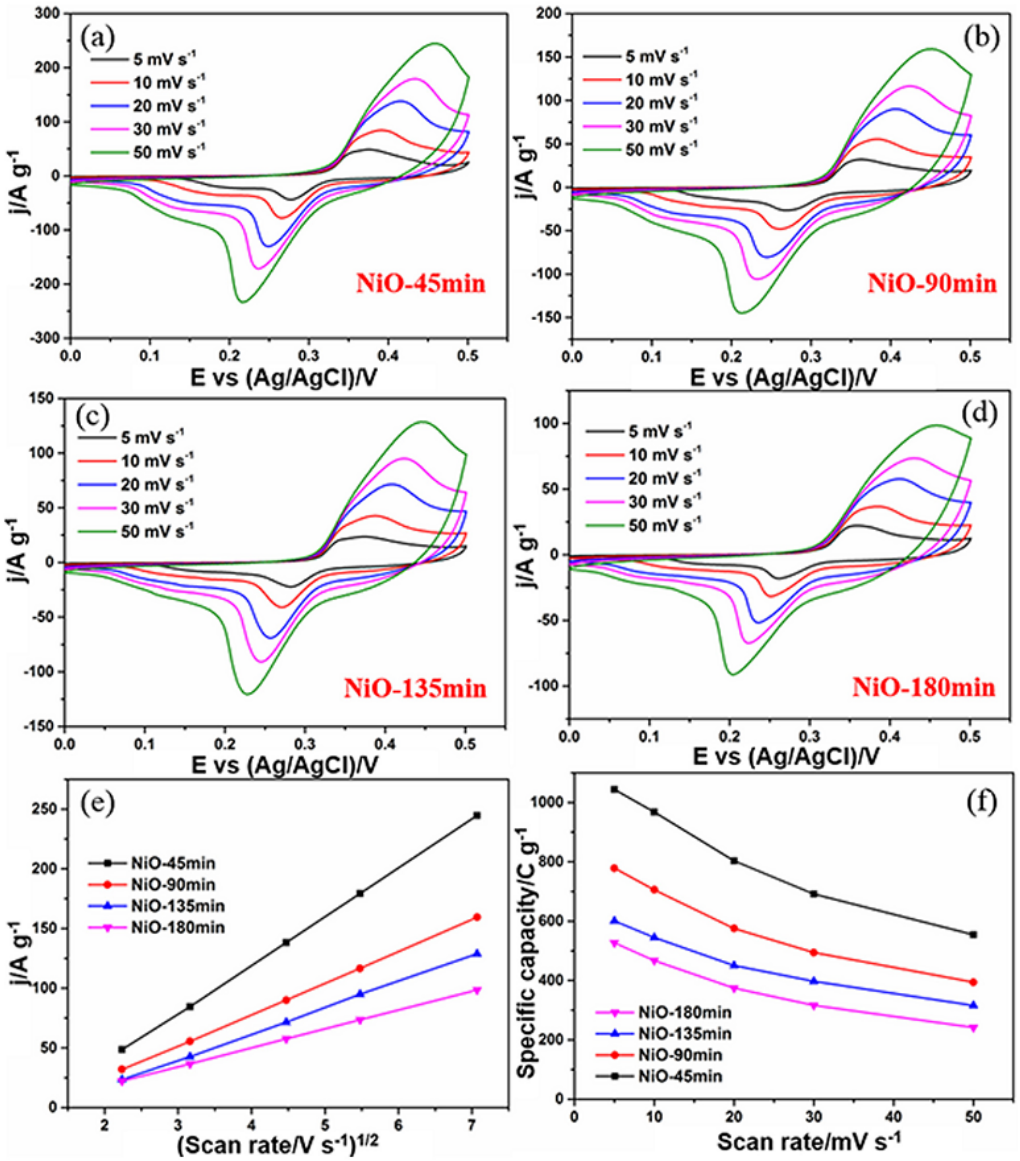

es at various scan rates of NiO/Ni foam electrodes prepared with the sparking times of (a) 45 min, (b) 90 min, (c) 135 min and (d) 180 min, (e) corresponding ırrent vs. the square root of scan rate plots and (f) corresponding specific capacity vs. scan rate plots.

g to the XPS analysis, the $Ni(OH)_2$ content decreases sing sparking time. Consequently, the contribution of decreases while that of reaction (2) increases as the ne increases. The change of these contributions may to the decreasing current density at a given scan rate sing sparking time as seen in Fig. 6 (a)-(d) because the e of $Ni(OH)_2$ should be relatively high compared with [34,57]. Regarding the effect of scan rate on peak an be observed that both of anodic and cathodic peak nift toward more positive and negative potentials, . This behavior can be attributed to the escalating of the istance of the electrode with increasing scan rate [57]. peak current is plotted with the square root of scan rate l in Fig. 6 (e). It is seen that all NiO/Ni foam electrodes exhibit linear relationships, demonstrating that the redox reactions at the sparked NiO surface is controlled by the diffusion of $[OH^-]$ [34]. In addition, the slope of peak current vs. the square root of scan rate increases with decreasing sparking time, indicating the higher electrocatalytic activity of the NiO/Ni foam electrode prepared with a shorter sparking time [34].

The performance of the sparked NiO on Ni foam as a battery-type electrode is characterized in term of the specific capacity (Q_{sp}, C g^{-1}) that can be calculated from CV curves according to [58,59]:

$$Q_{sp} = \frac{1}{\nu\, m}\int_{V_i}^{V_f} i\, dV \qquad (3)$$

where ν is the scan rate (V s^{-1}), m is a mass of the active material (g), V_i (V) is the starting potential and V_f is the final potential (V). In

addition, the average specific capacitance (C_{sp}, F g^{-1}) = $Q_{sp}\Delta V$ where $\Delta V \equiv V_f - V_i$ will also be reported here in order to allow direct comparisons with the results of several other published reports that mistakenly describe NiO and other similar materials as pseudocapacitors. Fig. 6 (f) shows the specific capacity vs. scan rate of NiO/Ni foam electrodes prepared with various sparking times. It is seen that Q_{sp} of all electrodes decrease monotonically with increasing scan rate, signifying the lower redox activity at a higher scan rate [60]. From above analysis, the redox reactions at NiO/Ni foam electrodes are diffusion-limited. Thus, the interfacial reaction kinetics are quite slow so that ionic/electronic movements in and out of NiO surfaces cannot respond the fast potential change at a higher scan rate, leading to a lower ion transfer rate, a thinner diffusion layer and lower charge capacity [61,62].

Moreover, it is evident that the charge capacity decreases monotonically with increasing sparking time and the NiO/Ni foam electrode produced with the shortest sparking time of 45 min exhibits the best charge storage performances with the highest and the lowest Q_{sp} (C_{sp}) values of ~1043 C g^{-1} (2087 F g^{-1}) at 5 mV s^{-1} and ~554 C g^{-1} (1109 F g^{-1}) at 50 mV s^{-1}, respectively. The effect can be explained based on the structural change observed by SEM and TEM that NiO nanoparticles become larger and aggregate into larger clusters loosely connected as a foam-like network with a large pore size as the sparking time increases, leading to a lower surface area for reactions with the alkaline electrolyte and a lower amount of charges generated through the redox reactions [3]. In addition, the NiO/Ni foam prepared at a shorter sparking time has higher contribution of more active $Ni(OH)_2$ species on surface (according to XPS data), resulting in further enhancement of faradaic reaction rates. Thus, the sparking time should be moderately short to optimize the porosity and chemical properties of sparked NiO layers on Ni foams. However, too short sparking time will lead to an incomplete coverage of NiO layer on Ni foam and a lower charge capacity. It has been found that 45 min is the shortest time that yields sufficiently complete NiO coverage on Ni foam and it is thus selected as the minimum sparking time. Moreover, the attained charge capacity (1043 C g^{-1} @5 mV s^{-1}) of the optimal electrode (NiO-45 min) is considerably better than other previously reported NiO-based electrodes having various morphologies prepared by different methods as listed in Table 1, which offered Q_{sp} values in the range of 162-548 C g^{-1} @1-5 mV s^{-1} [30,63].

Fig. 7 illustrates the GCD data of NiO/Ni foam electrodes prepared with different sparking times. The NiO/Ni foam electrodes are characterized by GCD. The GCD curves at various current densities of sparked NiO films with different sparking times (Fig. 7 (a)-(d)) show non-linear charge-discharge behaviors, confirming a battery-type charge storage mechanism of sparked NiO structures in accordance with the CV results. In addition, the charge and discharge times decrease more rapidly with increasing current density. The discharge profiles can be divided into three distinct regions. The first region (0.5-0.38 E Vs (Ag/AgCl)/V) begins with a rapid decay of potential with time, followed by a much slower discharge regime (0.38-0.28 E Vs (Ag/AgCl)/V) and the last section (0.28-0 E Vs (Ag/AgCl)/V) having a very fast potential drop behavior. The middle regime corresponds to the region of faradaic reaction peaks that generate the majority of stored charges while the other two regions contribute very small amounts of charges due to much lower redox reaction rates. To see the effect of sparking time on GCD behaviors, the GCD curves of sparked NiO/Ni foam electrodes with various sparking times are compared at a current density of 1 A g^{-1} as displayed in Fig. 7 (e). It is evident that the charge and discharge times decrease monotonically as the sparking time increases from 45 to 180 min, signifying the decrease of charge capacity in agreement with the CV results. The specific charge capacity, Q_{sp}, can be calculated from GCD curves according to:

$$Q_{sp} = \frac{It}{m} \quad (4)$$

where I is the discharge current (A), t is the discharge time (sec) and m is defined previously. Fig. 7 (f) shows the specific capacity vs. current density of NiO/Ni foam electrodes with different sparking times. It is apparent that the Q_{sp} value decreases monotonically with increasing current density, similar to the decreasing trend of CV-derived Q_{sp} with increasing scan rate (Fig. 6 (f)). In addition, the Q_{sp} values obtained from GCD are in the same range as the values calculated from CV. The amount of stored charges decreases at a higher current density because fewer ions can penetrate into the inner pore surfaces when the potential changes rapidly due to fast charging and discharging at a high current [60,64]. At the lowest current density of 1 A g^{-1}, NiO/Ni foam electrodes prepared with sparking times of 45, 90, 135 and 180 min exhibit high specific capacities of 920 C g^{-1} (1840 F g^{-1}), 745 C g^{-1} (1490 F g^{-1}), 475 C g^{-1} (950 F g^{-1}) and 360 C g^{-1} (720 F g^{-1}), respectively. When raising the current density from 1 A g^{-1} to 20 A g^{-1}, corresponding Q_{sp} values of the electrodes reduce to 76%, 62%, 51% and 39% of their highest values at 1 A g^{-1}, respectively. Thus, the NiO-45 min electrode exhibits not only higher specific capacity but also better discharge rate capability than other NiO/Ni foam electrodes. Furthermore, the achieved GCD performances (920 C g^{-1} @1 A g^{-1} and 699 (76% of 920) C g^{-1} @20 A g^{-1}) of NiO-45 min are also superior to other NiO-

Table 1
Charge storage performances of NiO-based electrodes prepared by various methods.

Materials	Methods	Q_{sp} (C g^{-1})	Cycling performance	Ref.
NiO thin film	Spray deposited	162@5 mV s^{-1}	92.1%@1 A g^{-1}, 1000 cycles	[29]
NiO thin film	Chemical precipitation	200.4@20 mV s^{-1}	Not report	[30]
NiO Nanotubes	Anodic aluminum oxide template	133@0.1 A g^{-1}	93%@0.1 A g^{-1}1000 cycles	[63]
NiO nanoflakes	Potentiodynamic deposition	133.2@0.1 mA cm^{-1}	94%@100 mV s^{-1} 1000 cycles	[64]
NiO hexagonal nanoplates	Surfactant self-assembly	129@1 A g^{-1}	88.5%@1 A g^{-1}, 1000 cycles	[65]
Hollow NiO nanofibers	Electrospinning	144.5@5 mA cm^{-1}	87%@5 mA cm^{-1}, 1000 cycles	[53]
Porous NiO nanowall arrays	Direct synthesis	148.5@0.67 A g^{-1}	93%@13.35 A g^{-1}, 4000 cycles	[66]
NiO nanoplatelets	Microwave method	548@1 mV s^{-1}, 780@1 A g^{-1}	98.5%@2 A g^{-1}, 1000 cycles	[33]
Porous NiO microflowers	Coordination of microflowers	755.1@0.625 A g^{-1}	99.7@6.25 A g^{-1}, 1000 cycles	[67]
NiO spherical spongy	Reflux	505@1 A g^{-1}	139.6%@4 A g^{-1}, 1000 cycles	[32]
NiO urchinlike	Hydrothermal	145@4 mA g^{-1}	99.7%@4 mA g^{-1}, 500 cycles	[68]
NiO flower-like microspheres	Hydrothermal	259@1 A g^{-1}	96%@15 A g^{-1}, 1000 cycles	[69]
NiO nanoparticles	Hydrothermal	476.3@1 A g^{-1}	62%@5 A g^{-1}, 3750 cycles	[31]
NiO nanoparticles on AU/PET sheets	Sparking method	402.7@1 A g^{-1}	88%@40 A g^{-1}, 1000 cycles	[34]
NiO nanoparticles on NiO foam	Sparking method	1043@5 mV s^{-1}, 920@1 A g^{-1}	96%@4 A g^{-1}, 1000 cycles	**This work**

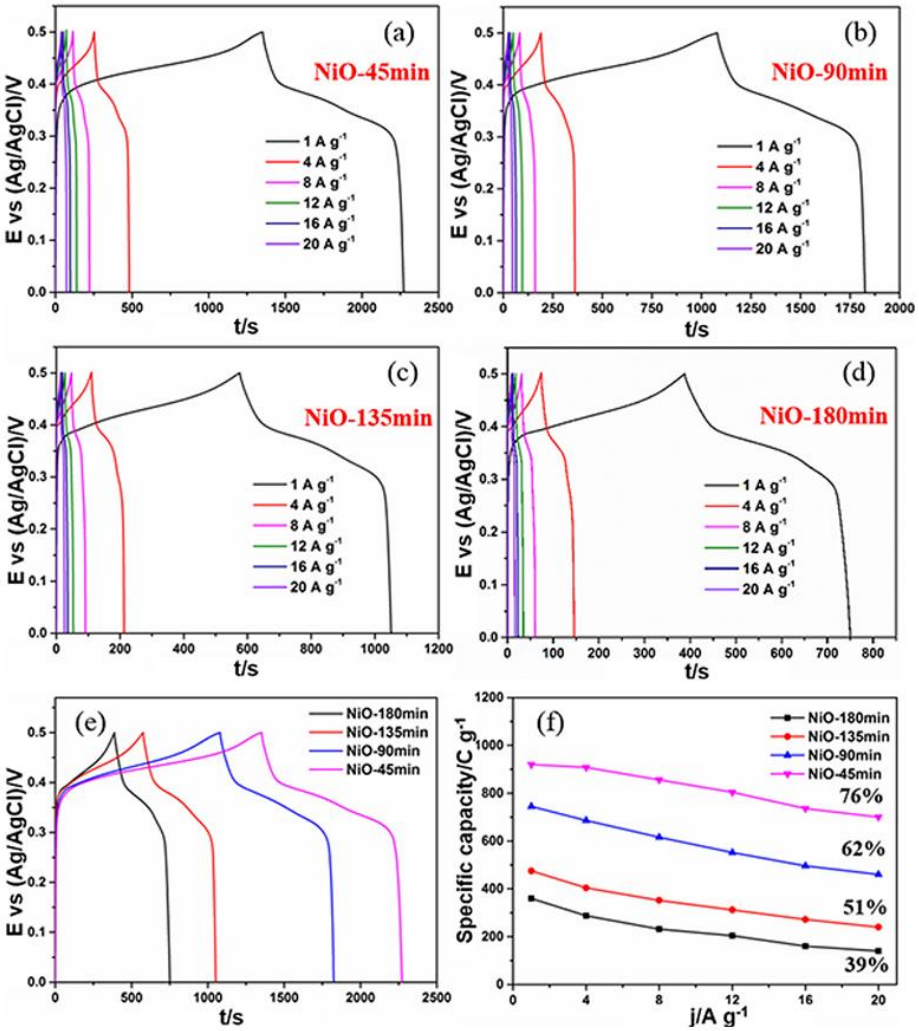

Fig. 7. GCD curves at various current densities of NiO/Ni foam electrodes prepared with the sparking times of (a) 45 min, (b) 90 min, (c) 135 min and (d) 180 min, (e) GCD curves at a current density of 1 A g^{-1} of sparked NiO films with varying sparking times and (f) the corresponding specific capacity vs. current density.

based electrodes as summarized previously in Table 1, which offered Q_{sp} values in the range of 129-755 C g^{-1} @0.1-1 A g^{-1} [65,66]. The efficacy of NiO/Ni foam electrode with the short sparking time of 45 min may be attributed to binder-free nanoporous morphology with very small particle and pore sizes as well as a low degree of agglomeration of NiO nanostructures, enhancing the faradaic process particularly the transportation and diffusion of ions/electrons between the active material and the alkaline electrolyte [67]. Moreover, the results are also substantially higher than the NiO nanoparticles sparked on planar Au/PET substrates (403 C g^{-1} @1 A g^{-1}) [35], demonstrating that 3D Ni foam substrates can significantly enhance the surface area of sparked NiO nanostructures.

Fig. 8 (a) illustrate the GDD profiles of NiO-45 min and NiO-180 min for 10 cycles of charging/discharging at 4 A g^{-1}. It is seen that both NiO/Ni foam electrodes display repeatable charging/discharging profiles in these 10 cycles. The corresponding specific charge capacity was calculated from the GCD profiles and plotted as a function of the cycle number up to 1000 as shown in Fig. 8 (b). From the results, the charge capacities of NiO-45 min and NiO-180 min increase gradually as the number of cycles rises from 0 to 100-150 up to ~110% and 103% of their starting values, respectively. This behavior may be attributed to the enhancement of surface wettability after the initial cycles via cycle induction [68], leading to higher electro-active NiO surface area for redox reactions [69]. As the cycle number increases further, the capacities of both electrodes decrease slowly and become quite steady at a large number of cycles (>900). At 1000 cycles, the NiO-45 min and NiO-180 min can retain ~96% and ~89% of specific capacities relative to their initial values. The better cycling performances of NiO-45 min

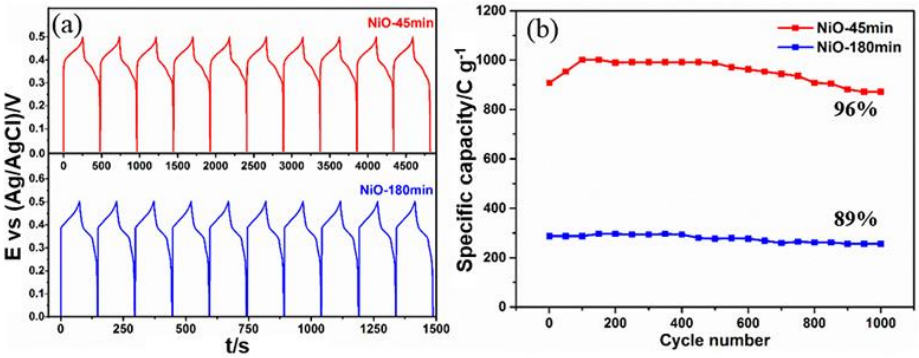

Fig. 8. (a) The first 10 cycles of GCD profiles at 4 A g^{-1} of NiO-45 min and NiO-180 min and (b) the corresponding cycling performance of specific capacity at 4 A g^{-1} up to 1000 cycles.

electrode may be related to the superior adhesion of thin sparked NiO layer on Ni foam compared with that of thicker one. From structural characterizations, the thicker sparked NiO layer contains more loosely agglomerated NiO nanoparticles with larger particle and pore sizes, which may be more easily detached from the structure by vigorous redox reaction leading to higher loss of capacity. The obtained cycling performances are better than or comparable with several other reports except a few as listed in Table 1. Therefore, the NiO/Ni foam electrode prepared by sparking method is highly attractive for electrochemical energy-storage applications because of its excellent charge capacity, rate capability and cycling performances as well as low cost, environmental friendly and simple fabrication process.

Fig. 9 demonstrates the EIS characteristics of sparked NiO/Ni foam electrodes with various sparking times. The observed impedance behaviors of the NiO-based electrodes may be described by two distinct mechanisms taking place in low and high frequency regions. In the low frequency region, the impedance displays a steep slope of 70-75°, which may be attributed to faradaic process at the NiO/Ni foam electrode, exhibiting a non-ideal capacitive behavior [70]. For the high frequency region, the impedance exhibits a smaller slope at an angle of 50-60°, signifying the process of ion diffusion into the porous NiO/Ni foam electrodes and the higher angle may imply the higher diffusion rate and lower charge transfer resistance due to the more porous structure of sparked NiO/Ni foam at a shorter sparking time [71]. The equivalent series resistance (ESR) can be determined from the intercept to the real part (Z') of impedance at high frequency (Inset). It is clear that the ESR value of NiO/Ni foam increases monotonically from 0.40 to 0.56 Ω as the sparking time increases from 45 to 180 min. For this structure, ESR is the total equivalent resistance, comprising the internal resistance of NiO layer as well as Ni foam, the ionic resistance of the electrolyte and the contact resistance between NiO and current collector (Ni foam) [29,71–73]. The lower ESR value at a shorter sparking time implies the lower internal resistance of sparked NiO layer, which should be due mainly to the smaller film thickness. Therefore, the superior electrochemical charge-storage properties of NiO-45 min observed from the CV and GCD data can also be related to the smaller internal and charge transfer resistances of the more porous and thinner sparked NiO layer.

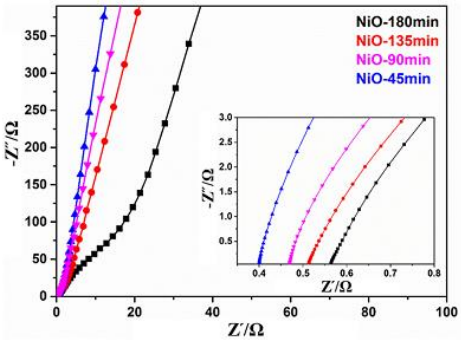

Fig. 9. Nyquist plots of sparked NiO/Ni foam electrodes with different sparking times.

4. Conclusions

In summary, the NiO/Ni foam electrodes were fabricated by a sparking method with varying sparking times from 45 to 180 min and systematically characterized for electrochemical energy storage applications. The structural characterizations by SEM, EDS, TEM, XPS and Raman spectroscopy revealed that the diameter of sparked NiO nanoparticles and the pore size of the porous NiO network simultaneously increased while the contribution of Ni $(OH)_2$ species on NiO surface decreased with increasing sparking time. From CV and GCD measurements, the optimal sparking time of 45 min resulted in the highest energy storage performances having high specific capacities of 920 C g^{-1} at 1 A g^{-1} and 699 (76% of 920) C g^{-1} at 20 A g^{-1} as well as a good cycling performance with 96% retention after 1000 cycles at a current density of 4 A g^{-1} and a low ESR of 0.4 Ω. The attained performances could be attributed to highly porous and very small NiO nanoparticles on large surface area 3D Ni foam structure as well as higher contribution of active $Ni(OH)_2$ surface species. Therefore, the optimized NiO/Ni foam electrode fabricated by the sparking method is a highly promising candidate for electrochemical energy storage applications.

Acknowledgements

The authors appreciatively acknowledge the financial support from Thailand Graduate Institute of Science and Technology (TGIST) (TG-44-10-55-012D), National Science and Technology Development Agency (NSTDA), National Research University (NRU) Project under the Office of the Higher Education Commission, Center of Advanced Materials for Printed Electronics and Sensors, Materials Science Research Center, Graduate School

Department of Physics and Materials Science, Faculty of Science, Chiang Mai University. Also, we are immensely grateful to Dr. Papawee Suabjakyong, National Institute of Advanced Industrial Science and Technology, Japan, Mrs. Budsabong Kuntalue, Electron Microscopy Research and Service Center, Faculty of Science, Chiang Mai University Mr. Tongkham Taya and Medical Science Research Equipment Center, Faculty of Medicine, Chiang Mai University for supporting the databases, helping with the TEM operation and providing a high-precision microbalance with 5 digit resolution (240A, Precisa). Moreover, the special thanks should be given to the National Electronics and Computer Technology Center (NECTEC), Pathumthani, Thailand and Research Laboratory for Analytical Instrument and Electrochemistry Innovation, Faculty of Science, Chiang Mai University for electrochemical test.

References

[1] X. Wu, Q. Wang, W. Zhang, Y. Wang, W. Chen, Nano nickel oxide coated graphene/polyaniline composite film with high electrochemical performance for flexible supercapacitor, Electrochimica Acta 211 (2016) 1066–1075.
[2] S.-I. Kim, J.-S. Lee, H.-J. Ahn, H.-K. Song, J.-H. Jang, Facile Route to an Efficient NiO Supercapacitor with a Three-Dimensional Nanonetwork Morphology, ACS Applied Materials & Interfaces 5 (2013) 1596–1603.
[3] J. Chen, J. Xu, S. Zhou, N. Zhao, C.-P. Wong, Amorphous nanostructured FeOOH and Co–Ni double hydroxides for high-performance aqueous asymmetric supercapacitors, Nano Energy 21 (2016) 145–153.
[4] P. Simon, Y. Gogotsi, B. Dunn, Where Do Batteries End and Supercapacitors Begin? Science 343 (2014) 1210.
[5] Y. Tao, L. Ruiyi, Y. Tingting, L. Zaijun, Nickel/cobalt layered double hydroxide hollow microspheres with hydrangea-like morphology for high-performance supercapacitors, Electrochimica Acta 152 (2015) 530–537.
[6] J. Chang, Z. Gao, X. Liu, D. Wu, F. Xu, Y. Guo, Y. Guo, K. Jiang, Hierarchically porous carbons with graphene incorporation for efficient supercapacitors, Electrochimica Acta 213 (2016) 382–392.
[7] Y. Han, N. Shen, S. Zhang, D. Li, X. Li, Fish gill-derived activated carbon for supercapacitor application, Journal of Alloys and Compounds 694 (2017) 636–642.
[8] A.M. Abioye, Z.A. Noorden, F.N. Ani, Synthesisand Characterizations of Electroless Oil Palm Shell Based-Activated Carbon/Nickel Oxide Nanocomposite Electrodes for Supercapacitor Applications, Electrochimica Acta.
[9] Y. Xie, L. Lu, Y. Tang, F. Zhang, C. Shen, X. Zang, X. Ding, W. Cai, L. Lin, Hierarchically nanostructured carbon fiber-nickel-carbon nanotubes for high-performance supercapacitor electrodes, Materials Letters 186 (2017) 70–73.
[10] Y.-Y. Ma, G.-B. Yi, J.-C. Wang, H. Wang, H.-S. Luo, X.-H. Zu, Shape-controllable and -tailorable multi-walled carbon nanotube/MnO2/shape-memory polyurethane composite film for supercapacitor, Synthetic Metals 223 (2017) 67–72.
[11] D. Yang, C. Bock, Laser reduced graphene for supercapacitor applications, Journal of Power Sources 337 (2017) 73–81.
[12] L. Lu, W. Li, L. Zhou, Y. Zhang, Z. Zhang, Y. Chen, J. Liu, L. Liu, W. Chen, Y. Zhang, Impact of size on energy storage performance of graphene based supercapacitor electrode, Electrochimica Acta 219 (2016) 463–469.
[13] T. Brousse, D. Bélanger, J.W. Long, To Be or Not To Be Pseudocapacitive? Journal of The Electrochemical Society 162 (2015) A5185–A5189.
[14] T. Liu, L. Finn, M. Yu, H. Wang, T. Zhai, X. Lu, Y. Tong, Y. Li, Polyaniline and Polypyrrole Pseudocapacitor Electrodes with Excellent Cycling Stability, Nano Letters 14 (2014) 2522–2527.
[15] S. Cho, K.-H. Shin, J. Jang, Enhanced Electrochemical Performance of Highly Porous Supercapacitor Electrodes Based on Solution Processed Polyaniline Thin Films, ACS Applied Materials & Interfaces 5 (2013) 9186–9193.
[16] L. Chen, J. Kang, Y. Hou, P. Liu, A. Hirata, M. Chen, High-energy-density nonaqueous MnO2@nanoporous gold based supercapacitors, J Mater Chem A 1 (2013) 9202–9207.
[17] K.M. Kim, J.H. Nam, Y.-G. Lee, W.I. Cho, J.M. Ko, Supercapacitive properties of electrodeposited RuO2 electrode in acrylic gel polymer electrolytes, Current Applied Physics 13 (2013) 1702–1706.
[18] J.W. Lee, T. Ahn, J.H. Kim, J.M. Ko, J.-D. Kim, Nanosheets based mesoporous NiO microspherical structures via facile and template-free method for high performance supercapacitors, Electrochimica Acta 56 (2011) 4849–4857.
[19] S. Kong, F. Yang, K. Cheng, T. Ouyang, K. Ye, G. Wang, D. Cao, In-situ growth of cobalt oxide nanoflakes from cobalt nanosheet on nickel foam for battery-type supercapacitors with high specific capacity, Journal of Electroanalytical Chemistry.
[20] N. Wang, Y. Zhang, T. Hu, Y. Zhao, C. Meng, Facile hydrothermal synthesis of ultrahigh-aspect-ratio V2O5 nanowires for high-performance supercapacitors, Current Applied Physics 15 (2015) 493–498.
[21] Q.H. Do, J. Smithyman, C. Zeng, C. Zhang, R. Liang, J.P. Zheng, Toward binder-free electrochemical capacitor electrodes of vanadium oxide-nanostructured carbon by supercritical fluid deposition: Precursor adsorption and conversion, and electrode performance, Journal of Power Sources 248 (2014) 1241–1247.
[22] J. Li, X. Liu, Preparation and characterization of α-MoO3 nanobelt and its application in supercapacitor, Materials Letters 112 (2013) 39–42.
[23] Y. Fu, J. Song, Y. Zhu, C. Cao, High-performance supercapacitor electrode based on amorphous mesoporous Ni(OH)2 nanoboxes, Journal of Power Sources 262 (2014) 344–348.
[24] M.-S. Wu, J.-F. Wu, Nickel hydroxide electrode with porous nanotube arrays prepared by hydrolysis and cathodic deposition for high-performance supercapacitors, Journal of Power Sources 240 (2013) 397–403.
[25] T. Zhao, H. Jiang, J. Ma, Surfactant-assisted electrochemical deposition of α-cobalt hydroxide for supercapacitors, Journal of Power Sources 196 (2011) 860–864.
[26] M. Suksomboon, P. Srimuk, A. Krittayavathananon, S. Luanwuthi, M. Sawangphruk, Effect of alkaline electrolytes on the charge storage capacity and morphology of porous layered double cobalt hydroxide-coated graphene supercapacitor electrodes, RSC Advances 4 (2014) 56876–56882.
[27] H. Wang, H. Yi, X. Chen, X. Wang, Facile synthesis of a nano-structured nickel oxide electrode with outstanding pseudocapacitive properties, Electrochimica Acta 105 (2013) 353–361.
[28] A. Jena, N. Munichandraiah, S.A. Shivashankar, Carbonaceous nickel oxide nano-composites: As electrode materials in electrochemical capacitor applications, Journal of Power Sources 237 (2013) 156–166.
[29] S. Xu, X. Li, Z. Yang, T. Wang, M. Xu, L. Zhang, C. Yang, N. Hu, D. He, Y. Zhang, A novel Ni@Ni(OH)2 coaxial core-sheath nanowire membrane for electrochemical energy storage electrodes with high volumetric capacity and excellent rate capability, Electrochimica Acta 182 (2015) 464–473.
[30] A.A. Yadav, U.J. Chavan, Influence of substrate temperature on electrochemical supercapacitive performance of spray deposited nickel oxide thin films, Journal of Electroanalytical Chemistry 782 (2016) 36–42.
[31] U.M. Patil, R.R. Salunkhe, K.V. Gurav, C.D. Lokhande, Chemically deposited nanocrystalline NiO thin films for supercapacitor application, Applied Surface Science 255 (2008) 2603–2607.
[32] G. Cheng, Y. Yan, R. Chen, From Ni-based nanoprecursors to NiO nanostructures: morphology-controlled synthesis and structure-dependent electrochemical behavior, New Journal of Chemistry 39 (2015) 676–682.
[33] M. Liu, J. Chang, J. Sun, L. Gao, Synthesis of porous NiO using NaBH4 dissolved in ethylene glycol as precipitant for high-performance supercapacitor, Electrochimica Acta 107 (2013) 9–15.
[34] M. Khairy, S.A. El-Safty, Mesoporous NiO nanoarchitectures for electrochemical energy storage: influence of size, porosity, and morphology, RSC Advances 3 (2013) 23801–23809.
[35] Y. Chuminjak, S. Daothong, P. Reanpang, J.P. Mensing, D. Phokharatkul, J. Jakmunee, A. Wisitsoraat, A. Tuantranont, P. Singjai, Electrochemical energy-storage performances of nickel oxide films prepared by a sparking method, RSC Advances 5 (2015) 67795–67802.
[36] K. Inyawilert, A. Wisitsora-at, A. Tuantranont, P. Singjai, S. Phanichphant, C. Liewhiran, Ultra-rapid VOCs sensors based on sparked-In2O3 sensing films, Sensors and Actuators B: Chemical 192 (2014) 745–754.
[37] W. Thongsuwan, T. Kumpika, P. Singjai, Photocatalytic property of colloidal TiO2 nanoparticles prepared by sparking process, Current Applied Physics 8 (2008) 563–568.
[38] W. Thongsuwan, T. Kumpika, P. Singjai, Effect of high roughness on a long aging time of superhydrophilic TiO2 nanoparticle thin films, Current Applied Physics 11 (2011) 1237–1242.
[39] T. Kumpika, W. Thongsuwan, P. Singjai, Atomic force microscopy imaging of ZnO nanodots deposited on quartz by sparking off different tip shapes, Surface and Interface Analysis 39 (2007) 58–63.
[40] K. Hongsith, N. Hongsith, D. Wongratanaphisan, A. Gardchareon, S. Phadungdhitidhada, P. Singjai, S. Choopun, Sparking deposited ZnO nanoparticles as double-layered photoelectrode in ZnO dye-sensitized solar cell, Thin Solid Films 539 (2013) 260–266.
[41] L. Wang, X. Li, T. Guo, X. Yan, B.K. Tay, Three-dimensional Ni(OH)2 nanoflakes/graphene/nickel foam electrode with high rate capability for supercapacitor applications, International Journal of Hydrogen Energy 39 (2014) 7876–7884.
[42] K. Bhagaban, R. Patta, D. Arnab, A. Srinivasan, A. Perumal, Structural, vibrational, optical and magnetic properties of NiO nanoparticles, Science Letters Journal 4 (2015) 160.
[43] M. Zhou, H. Chai, D. Jia, W. Zhou, The glucose-assisted synthesis of a graphene nanosheet-NiO composite for high-performance supercapacitors, New Journal of Chemistry 38 (2014) 2320–2326.
[44] N. Mironova-Ulmane, A. Kuzmin, I. Steins, J. Grabis, I. Sildos, M. Pärs, Raman scattering in nanosized nickel oxide NiO, Journal of Physics: Conference Series 93 (2007) 012039.
[45] W.J. Duan, S.H. Lu, Z.L. Wu, Y.S. Wang, Size Effects on Properties of NiO Nanoparticles Grown in Alkalisalts, The Journal of Physical Chemistry C 116 (2012) 26043–26051.
[46] C. Yuan, J. Li, L. Hou, X. Zhang, L. Shen, X.W. Lou, Ultrathin Mesoporous NiCo2O4 Nanosheets Supported on Ni Foam as Advanced Electrodes for Supercapacitors, Advanced Functional Materials 22 (2012) 4592–4597.
[47] L. Yu, G. Wang, G. Wan, G. Wang, S. Lin, X. Li, K. Wang, Z. Bai, Y. Xiang, Highly effective synthesis of NiO/CNT nanohybrids by atomic layer deposition for high-rate and long-life supercapacitors, Dalton Transactions 45 (2016) 13779–13786.
[48] J.-z. Huang, Z. Xu, H.-l. Li, G.-h. Kang, W.-j. Wang, Influence of process parameters on electrochemical and physical properties of sputtered iron-doped nickel oxide thin films, Transactions of Nonferrous Metals Society of China 16 (2006) 1301–1306.

[49] M.V. Bykova, D.Y. Ermakov, V.V. Kaichev, O.A. Bulavchenko, A.A. Saraev, M.Y. Lebedev, V.A. Yakovlev, Ni-based sol–gel catalysts as promising systems for crude bio-oil upgrading: Guaiacol hydrodeoxygenation study, Applied Catalysis B: Environmental 113–114 (2012) 296–307.
[50] J.B. Wu, R.Q. Guo, X.H. Huang, Y. Lin, Construction of self-supported porous TiO2/NiO core/shell nanorod arrays for electrochemical capacitor application, Journal of Power Sources 243 (2013) 317–322.
[51] A. Shanmugavani, R.K. Selvan, Microwave assisted reflux synthesis of NiCo2O4/NiO composite: Fabrication of high performance asymmetric supercapacitor with Fe2O3, Electrochimica Acta 189 (2016) 283–294.
[52] X. Feng, N. Dementev, W. Feng, R. Vidic, E. Borguet, Detection of low concentration oxygen containing functional groups on activated carbon fiber surfaces through fluorescent labeling, Carbon 44 (2006) 1203–1209.
[53] C. Yuan, J. Li, L. Hou, L. Yang, L. Shen, X. Zhang, Facile growth of hexagonal NiO nanoplatelet arrays assembled by mesoporous nanosheets on Ni foam towards high-performance electrochemical capacitors, Electrochimica Acta 78 (2012) 532–538.
[54] B. Ren, M. Fan, Q. Liu, J. Wang, D. Song, X. Bai, Hollow NiO nanofibers modified by citric acid and the performances as supercapacitor electrode, Electrochimica Acta 92 (2013) 197–204.
[55] Y. Wang, S. Gai, C. Li, F. He, M. Zhang, Y. Yan, P. Yang, Controlled synthesis and enhanced supercapacitor performance of uniform pompon-like β-Ni(OH)2 hollow microspheres, Electrochimica Acta 90 (2013) 673–681.
[56] L. Zhang, K.N. Hui, K. San Hui, H. Lee, High-performance hybrid supercapacitor with 3D hierarchical porous flower-like layered double hydroxide grown on nickel foam as binder-free electrode, Journal of Power Sources 318 (2016) 76–85.
[57] Y. Zhu, C. Cao, S. Tao, W. Chu, Z. Wu, Y. Li, Ultrathin Nickel Hydroxide and Oxide Nanosheets: Synthesis, Characterizations and Excellent Supercapacitor Performances, Scientific Reports 4 (2014) 5787.
[58] S.K. Meher, P. Justin, G. Ranga Rao, Microwave-Mediated Synthesis for Improved Morphology and Pseudocapacitance Performance of Nickel Oxide, ACS Applied Materials & Interfaces 3 (2011) 2063–2073.
[59] S.K. Meher, P. Justin, G.R. Rao, Pine-cone morphology and pseudocapacitive behavior of nanoporous nickel oxide, Electrochimica Acta 55 (2010) 8388–8396.
[60] S.T. Senthilkumar, R.K. Selvan, Y.S. Lee, J.S. Melo, Electric double layer capacitor and its improved specific capacitance using redox additive electrolyte, Journal of Materials Chemistry A 1 (2013) 1086–1095.
[61] R.G. Compton, C.E. Banks, Cyclic voltammetry at macroelectrodes:In understanding voltammetry, World Scientific, Singapore, 2007.
[62] F. Dar, K. Moonooswamy, M. Es-Souni, Morphology and property control of NiO nanostructures for supercapacitor applications, Nanoscale Research Letters 8 (2013) 363.
[63] D.S. Patil, S.A. Pawar, S.K. Patil, P.P. Salavi, S.S. Kolekar, R.S. Devan, Y.R. Ma, J.H. Kim, J.C. Shin, P.S. Patil, Electrochemical performance of potentiodynamically deposited polyaniline electrodes in ionic liquid, Journal of Alloys and Compounds 646 (2015) 1089–1095.
[64] F.I. Dar, K.R. Moonooswamy, M. Es-Souni, Morphology and property control of NiO nanostructures for supercapacitor applications, Nanoscale Res Lett 8 (2013).
[65] Z. Zhu, J. Ping, X. Huang, J. Hu, Q. Chen, X. Ji, C.E. Banks, Hexagonal nickel oxide nanoplate-based electrochemical supercapacitor, Journal of Materials Science 47 (2012) 503–507.
[66] H. Pang, Y. Shi, J. Du, Y. Ma, G. Li, J. Chen, J. Zhang, H. Zheng, B. Yuan, Porous nickel oxide microflowers synthesized by calcination of coordination microflowers and their applications as glutathione electrochemical sensor and supercapacitors, Electrochimica Acta 85 (2012) 256–262.
[67] H. Wang, Y. Wang, X. Wang, Pulsed laser deposition of the porous nickel oxide thin film at room temperature for high-rate pseudocapacitive energy storage, Electrochemistry Communications 18 (2012) 92–95.
[68] H. Wang, C.M.B. Holt, Z. Li, X. Tan, B.S. Amirkhiz, Z. Xu, B.C. Olsen, T. Stephenson, D. Mitlin, Graphene-nickel cobaltite nanocomposite asymmetrical supercapacitor with commercial level mass loading, Nano research 5 (2012) 605–617.
[69] J. Zhou, J. Lian, L. Hou, J. Zhang, H. Gou, M. Xia, Y. Zhao, T.A. Strobel, L. Tao, F. Gao, Ultrahigh volumetric capacitance and cyclic stability of fluorine and nitrogen co-doped carbon microspheres, Nature Communications 6 (2015) 8503.
[70] L. Li, Z. Dai, Y. Zhang, J. Yang, W. Huang, X. Dong, Carbon@NiCo2S4 nanorods: an excellent electrode material for supercapacitors, RSC Advances 5 (2015) 83408–83414.
[71] X. Meng, M. Feng, H. Zhang, Z. Ma, C. Zhang, Solvothermal synthesis of cobalt/nickel layered double hydroxides for energy storage devices, Journal of Alloys and Compounds 695 (2017) 3522–3529.
[72] M.-S. Wu, M.-J. Wang, J.-J. Jow, Fabrication of porous nickel oxide film with open macropores by electrophoresis and electrodeposition for electrochemical capacitors, Journal of Power Sources 195 (2010) 3950–3955.
[73] N. Duraisamy, A. Numan, S.O. Fatin, K. Ramesh, S. Ramesh, Facile sonochemical synthesis of nanostructured NiO with different particle sizes and its electrochemical properties for supercapacitor application, Journal of Colloid and Interface Science 471 (2016) 136–144.

CURRICULUM VITAE

Name Miss Yaowamarn Chuminjak

Date of birth 5 June 1986

Education
2005-2009 B.Sc. (Materials Science), Chiang Mai University
2009-2011 M.Sc. (Materials Science), Chiang Mai University
2011-2017 Ph.D. candidate (Materials Science), Chiang Mai University

Scholarship 2012-present Scholarship from Nanoscience and Nanotechnology Center, faculty of Science, Chiang Mai University Scholarship under Thailand Graduate Institute of Science and Technology (TGIST)

Conferences
-Y. Chuminjak, P. Singjai, Preparation of multiwall Carbon Nanotube films by electrophoretic Deposition, The 2nd CMU Graduate Research Conference, Chiang Mai, Thailand, 2010.
-Y. Chuminjak, P. Singjai, NiO nanoparticles Synthesis by sparking method, the 30th MST Annual Conference, Thailand, 2013.
-Y. Chuminjak, P. Singjai, Facile Synthesis and Characterization of Nanostructured Manganese Oxides,the 31th MST Annual Conference, Thailand, 2014.

Publications
-Y. Chuminjak,S. Daothong, P. Reanpang, J. P. Mensing,D. Phokharatkul, J. Jakmunee, A. Wisitsoraat, A. Tuantranont and P. Singjai, Electrochemical energy-storage performances of nickel oxide films prepared by a sparking method, RSC Advances, 2015; 5: 67795-67802.

-Y. Chuminjak, S. Daothong, A. Kuntarug, D. Phokharatkul, M. Horprathum, A. Wisitsoraat, A. Tuantranont, J. Jakmunee, and P. Singjai, High-performance Electrochemical Energy Storage Electrodes Based on Nickel Oxide-coated Nickel Foam Prepared by Sparking Method, Electrochimica Acta, 2017; 238: 298-309.